Sensors and Actuators: A. Physical 335 (2022) 113391

Contents lists available at ScienceDirect

Sensors and Actuators: A. Physical

journal homepage: www.elsevier.com/locate/sna

Parametric optimization of surface dielectric barrier discharge actuators for ice sensing application

M. Abdollahzadeh[a,*], F. Rodrigues[a,*], J. Nunes-Pereira[a,b], J.C. Pascoa[a,*], L. Pires[a]

[a] C-MAST, Centre for Mechanical and Aerospace Sciences and Technologies, Faculdade de Engenharia Eletromecânica, Universidade da Beira Interior, Rua Marquês d'Ávila e Bolama, 6201-001 Covilhã, Portugal
[b] CF-UM-UP, Centro de Física das Universidades do Minho e do Porto, Campus de Gualtar, 4710-057 Braga, Portugal

ARTICLE INFO

Article history:
Received 14 October 2021
Received in revised form 1 January 2022
Accepted 18 January 2022
Available online 21 January 2022

Keywords:
Ice sensing
Deicing
Thermal characterization
Experiments
Plasma actuator

ABSTRACT

In this paper a parametric optimization of the dielectric barrier discharge (DBD) plasma actuator is conducted in order to achieve better ice sensing and deicing performance. For this purpose, different DBD plasma actuators were tested by changing the main geometrical dimension of the DBD plasma actuator and dielectric material. Both the ice sensing and thermal characteristics of the DBD plasma actuator were analyzed and compared. The results reveal that there exists two separate set of optimum parameters that lead to best ice sensing and thermal behavior. For both the sensing and thermal characteristics, the thinnest DBD showed the best performance. Kapton DBD plasma actuator showed the highest surface temperature while PMMA (poly methyl methacrylate) had the best performance for ice sensing. In the end, the deicing performance of a DBD actuator that had in average better thermal and ice sensing performance was tested for deicing an ice layer and a frost layer. The progress of the deicing process and the ice sensing measure on the surface were recorded and analyzed.

1. Introduction

Controlling the surface icing event is a crucial part of the design of the aircraft and wind turbines that must operate in cold climates. For an aircraft ice accretion on the surface will change the aerodynamic performance of the wings and will change the drag and lift profile of the aircraft in a way that fuel consumption issues, and dangerous flight control problems may occur [1]. For cold climate wind turbines, accumulation of ice on the blades will increase the load and drag, leading to a reduction of the output power production of the wind turbines, and may also pose some structural damages [2]. As a solution to the above-mentioned problems, active ice control systems are being developed for aircraft and wind turbines.

One of the newest ice control systems has been developed based on DBD (dielectric barrier discharge) plasma actuators [3]. These devices are capable of increasing the surface temperature in a way that anti-icing or de-icing of a surface can be achieved. Tirumala et al. [4] and Rodrigues et al. [5,6] experimentally characterized the surface temperature of DBD plasma actuators by means of infrared thermographic measurements and demonstrated the fast surface temperature increase due to the plasma discharge operation. In addition, these devices are capable of controlling the flow near the surface where they are mounted and thus, are able to be used as flow control systems when deicing performance is not needed [7,8]. Considering these abilities, several authors started to study the operation of DBD plasma actuators for coupled flow control and ice accumulation prevention. Cai et al. [9] and Zhou et al. [10] performed experimental studies in icing wind tunnel and demonstrated that the thermal effect produced by the DBD plasma actuators is effective on preventing the ice accretion over cylinders or airfoils surfaces. In addition, Liu et al. [11] demonstrated, also by means of icing wind tunnel experiments, that DBD plasma actuators, when optimized with duty-cycle modulation, present much better anti-/de-icing performance than the conventional electrical heating method. Recently Meng et al. [12] studied the physical mechanism of coupled aerodynamic and thermal effects produced by a multi-SDBD (single dielectric barrier discharge) plasma actuator mounted on a NACA 0012 airfoil using different designs. The experiments were conducted in an icing-wind-tunnel, and they demonstrated that when the flow induced by the actuator is consistent with the incoming flow, the local temperature is higher and it could ensure that 57% of the chord of the airfoil lower surface was free of ice. When the plasma induced flow is produced in an opposite direction to the

* Corresponding authors.
E-mail addresses: mm.abdollahzadeh@ubi.pt (M. Abdollahzadeh), fmfr@ubi.pt (F. Rodrigues), pascoa@ubi.pt (J.C. Pascoa).

https://doi.org/10.1016/j.sna.2022.113391
0924-4247/

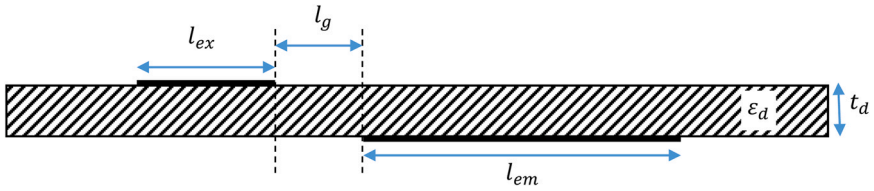

Fig. 1. Schematic of the DBD plasma actuators characteristic dimensions.

incoming flow, the local surface temperature is lower, but the ice accumulation was avoided in 81% of the chord of the airfoil lower surface. In addition, they verified that when the plasma flow is induced in a perpendicular direction to the incoming flow, the actuator presents higher local temperature and there is no ice accumulation on the entire lower surface of the airfoil. To improve the ice prevention ability, Kolbakir et al. [13] and Zheng et al. [14] proposed the use of a hybrid system combining the plasma actuator deicing effect with a hydrophobic surface effect. They concluded that, by combining both effects, the plasma actuators prevent the ice formation by inducing thermal effects while the hydrophobic surface provides lower adhesion and quick surface water runback.

In situations that the ice formation cannot be completely mitigated, the plasma flow control ability may be also used to avoid the formation of undesirable aerodynamic effects created by icing accumulation [15,16]. These actuators also have showed promising results in controlling separated flow around the blades of wind turbines [17], propulsion systems [18] and turbulent boundary layer flow control. Pouryoussefi et al. [19] demonstrated that plasma actuators also have an important role on controlling the separation bubble generated by the ice formation. They studied the operation of DBD plasma actuators on an iced airfoil NACA 203012, for angles of attack close to stall and post-stall, and verified that by activating the actuator the maximum lift coefficient of the iced airfoil increases about 6%. In addition, they verified that for an angle of attack of 16° the airfoil lift to drag aerodynamic ratio was increased about 100%. Considering this, they concluded that the plasma flow control effect may be used to considerably reduce the undesirable aerodynamic effects created by ice accumulation.

More interestingly, these actuators have proven to have a third characteristic which is the ability to detect the presence of ice on the surface based on measuring the variation in electric field. This ability was recently disclosed in Abdollahzadeh et al. [20,21], in which the authors demonstrated that the presence of air, water or ice on the actuator surface leads to changes in the electric field distribution and, thus, in the device electrical characteristics. By monitoring these changes, the plasma device can operate as an ice sensor allowing to identify the medium on its surface. After that, Rodrigues et al. [22] introduced the possibility of using segmented plasma actuators to perform ice detection in wider surfaces which, besides the detection of the ice, allows to identify the location where it is accumulating.

Until now, there is not any previous work regarding the possible influence of the main designing parameters of the DBD plasma actuators on ice sensing and ice control. To ensure that plasma actuators operate effectively as ice sensor, it is important to understand the influence of dielectric material and designing parameters on the device sensibility to detect the ice. In this paper, we aim to present a systematic study on the influence of various geometrical parameters and the dielectric material of the DBD plasma actuators for achieving better ice control capability. This paper is arranged as follows. In Section 1, a brief literature review regarding the application and progress of the DBD plasma actuators as icing control system is presented. In Section 2, the experimental setup and procedure used to conduct the present work is described. In Section 3, the problem and the main parameters involved are defined. In Section 4, the results for ice sensing and thermal characterization of DBD plasma actuators are presented. Finally, in the last section the main conclusion of the present work is summarized.

2. Problem definition

The main important geometrical parameter of a surface DBD includes the width of exposed electrode (l_{ex}), width of embedded electrode (l_{em}), the asymmetric gap between the electrodes (l_g) and thickness of dielectric layer (t_d). These geometrical parameters can be optimized to result in a better ice sensing performance and thermal characteristics that make the DBD plasma actuators more suitable as an ice control systemFig. 1.

Commercial dielectric materials exist in different pre-defined thickness. Therefore, the dielectric material also must be considered together with the parameter of the thickness of the dielectric layer. Kapton tapes exists in the market with very small thicknesses, for example 60 μm which allows easy fabrication of thicker dielectrics by layering Kapton tapes on each other. However, materials such as PIB rubber, PMMA comes normally with larger minimum thickness than Kapton, which limits the range of the dielectric thickness that can be produced from them. The reference values for the parameters of exposed electrode width, embedded electrode width, gap length, thickness of dielectric layer and the dielectric material are respectively as follows: 10 mm, 10 mm, 0 mm, 1 mm, Kapton. In the following sections we present the sensing and thermal characterization of various DBD actuators by varying the above-mentioned parameters. For all the test cases, the spanwise length of the DBD actuator was 4 cm. Normally the indicating parameters of plasma actuators are given as per spanwise length meaning that the mechanical behavior (induced flow) and thermal behavior can be essentially assumed uniform in the spanwise direction for enough long DBD actuators.

3. Experimental setup and procedure

Each of the fabricated DBD plasma actuators (with different dimensions and dielectric materials) were analyzed experimentally for their performance in ice sensing and deicing (thermal characteristics). In all the experimental tests, the DBD plasma actuators were operated by using an AC high voltage power source model *PVM 500*.

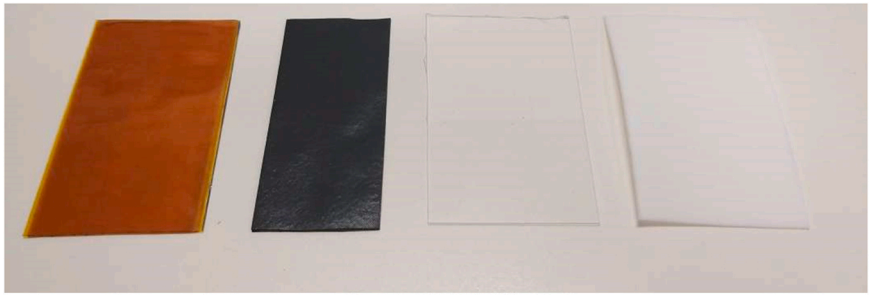

Kapton ($\varepsilon_d = 3.2$) PIB rubber ($\varepsilon_d = 2.82$) PMMA ($\varepsilon_d = 3$) Teflon ($\varepsilon_d = 2.1$)

Fig. 2. Dielectric layers with thickness of 1 mm made from different materials.

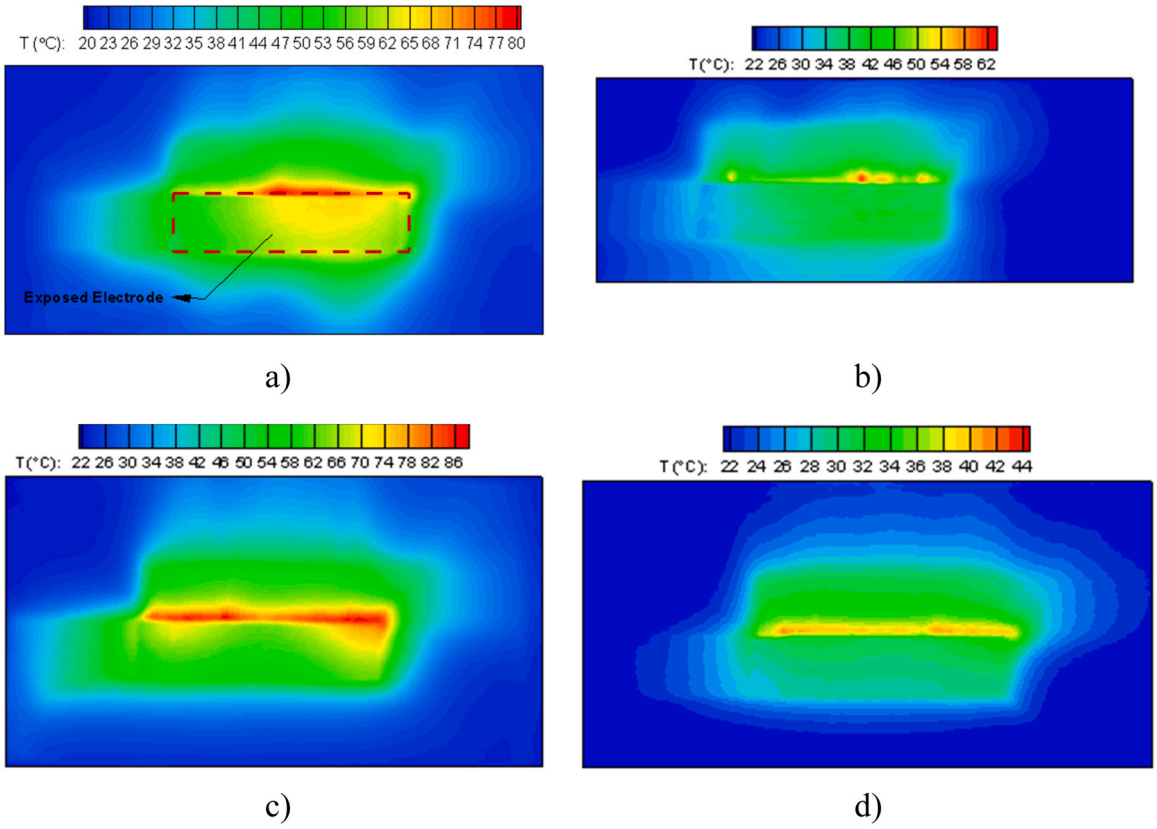

Fig. 3. Contour of surface temperature of the DBD plasma actuator operating at 8 kVpp for a) Kapton b) PIB rubber c) PMMA d) Teflon.

3.1. Ice sensing experiments

For obtaining a measure of ice sensing capability of DBD plasma actuators, their electrical characterization following a Lissajous charge-voltage diagram was conducted [23]. In this procedure, a monitoring capacitor was mounted in series with the DBD actuator and connected to the embedded electrode and the variation of the stored charge or its capacitance was monitored during the experiment with/without the presence of ice. The monitor capacitor consisted of a ceramic capacitor with a capacitance of 10 nF and a tolerance of 10%. The input voltage applied to the actuator and the voltage across the monitor capacitor was experimentally measured by using a digital oscilloscope model *Picoscope 5443 A*. The instantaneous charge of the capacitor Q_M is given by:

$$Q_M(t) = C_M \times V_M(t) \tag{1}$$

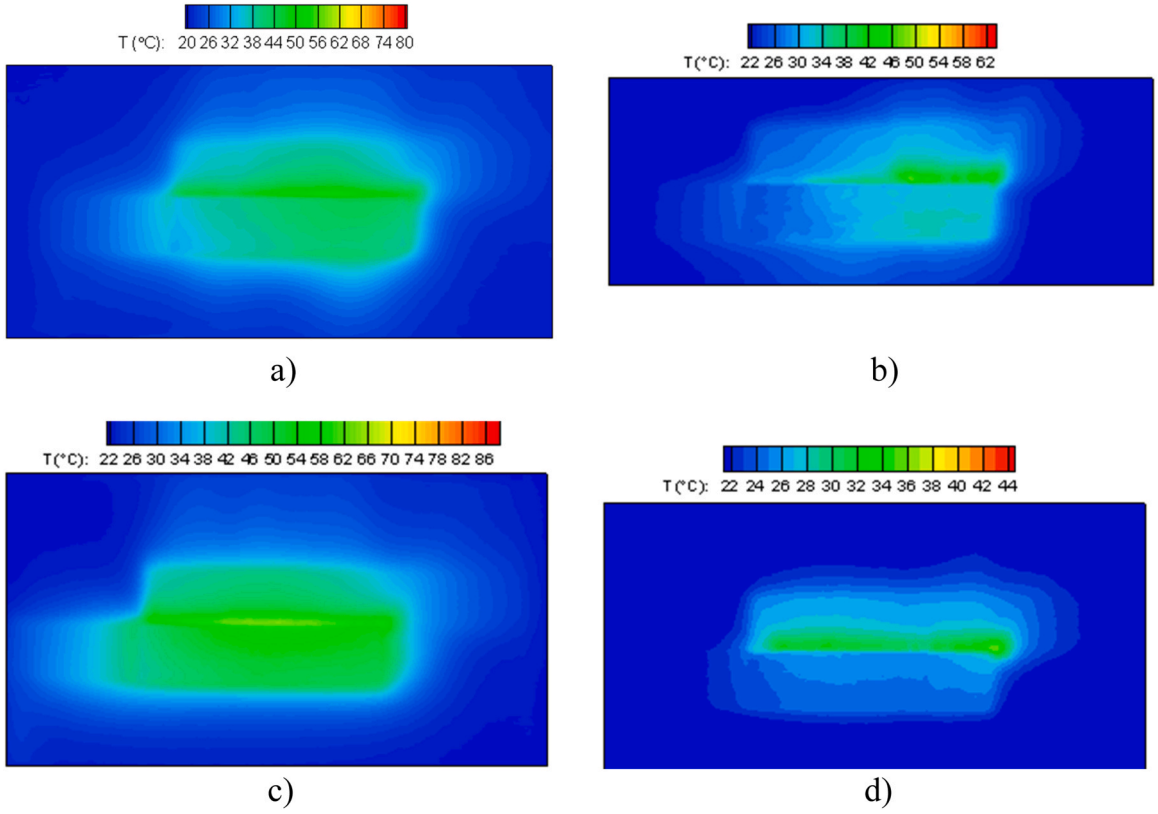

Fig. 4. Contour of surface temperature of the DBD plasma actuator operating at 7 kVpp for a) Kapton b) PIB rubber c) PMMA d) Teflon.

Where, V_M is the voltage across the capacitor and $C_M$is the capacitance. With the calculation of the instantaneous charge Q_M, its maximum measured value q_{max} can be calculated.

In the present work, an ice cube with dimensions $2 \times 2.5 \times 3cm^3$ was used as an ice sample and the electrical characterization of the actuator was measured with/without the ice cube on the surface. For each condition, tests were repeated 5 times and the average values of the maximum charge seen by the monitoring capacitor reported. The ratio of the maximum charge in the presence of ice to the maximum charge without the ice cube gives a measure about the sensitivity of the actuator to the presence of ice. Thus, the ice sensitivity can be defined as:

$$ice\ sensitivity\ (\%) = \frac{q_{max,with\ \ ice} - q_{max,no\ \ ice}}{q_{max,no\ \ ice}} \times 100\% \quad (2)$$

3.2. Thermal characterization

For the thermal characterization, the surface of the fabricated DBD plasma actuators were painted black ($\varepsilon = 0.98$) to allow accurate measurement of the surface temperature using infrared thermal imaging camera. By doing this, all the actuator surface presents the same emissivity and since we are using a matte black ink with high emissivity the contribution of surrounding reflections to the uncertainty of the measurements is negligible. In addition, a validation was performed in our previous work [24] in order to ensure that the thin black paint film does not influence the thermal behavior of the tested actuators. Before each measurement the DBD plasma actuator was operated at the desired voltage for 3 min. According with the literature, this time is sufficient to reach steady state surface

Table 1
Maximum and average temperatures induced by the operation of the DBD plasma actuators with different dielectric materials.

Material	Operating voltage							
	5 kVpp		6 kVpp		7 kVpp		8 kVpp	
	T_{avg}(°C)	T_{max}(°C)	T_{avg}(°C)	T_{max}(°C)	T_{avg}(°C)	T_{max}(°C)	T_{avg}(°C)	T_{max}(°C)
PIB rubber ($\varepsilon_d = 2.82$)	18.99	22.76	19.68	28.00	24.55	47.33	28.06	61.70
Kapton ($\varepsilon_d = 3.2$)	21.50	29.22	23.47	37.50	27.49	53.31	34.72	78.89
PMMA ($\varepsilon_d = 3$)	22.98	31.29	26.34	45.92	31.40	64.24	38.01	87.03
Teflon ($\varepsilon_d = 2.1$)	19.75	22.90	20.53	28.00	22.02	36.03	24.47	41.37

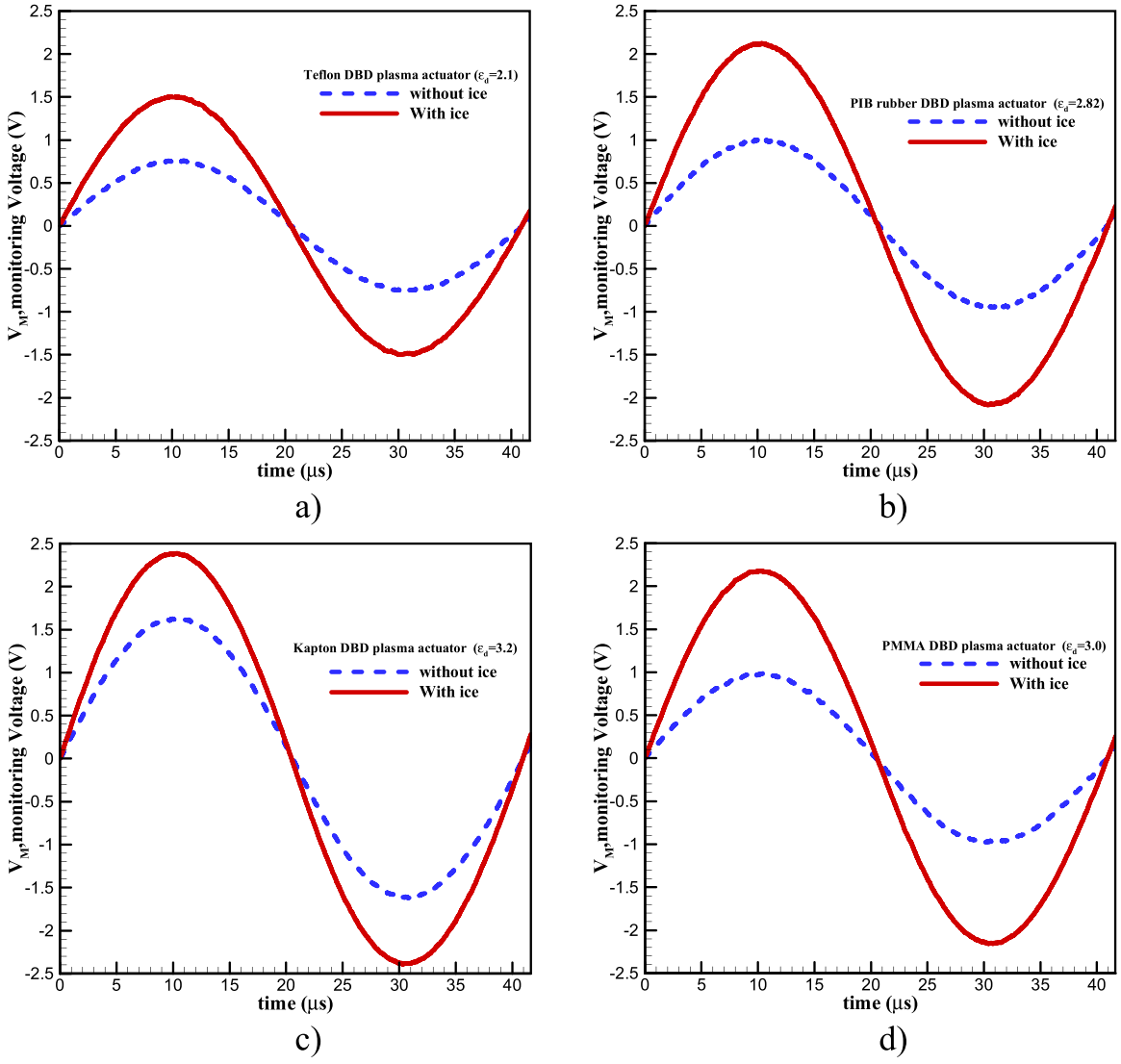

Fig. 5. Variation of the measured monitoring voltage at 4 kVpp and 24 kHz for the DBD plasma actuators with/without the presence of ice cube a) Teflon b) PIB rubber c) Kapton and d) PMMA.

temperature [4]. The surface temperature measurements were performed with an infrared thermal camera model *FLIR E50*. This infrared thermal camera presents a resolution of 240 × 180 pixels, a thermal sensitivity of less than 0.05 °C and an accuracy of ± 2%.

3.3. Deicing tests

After analyzing the best parameters and materials in terms of thermal and sensing characteristics, the plasma actuator was tested for coupled deicing and ice sensing application. An ice layer with constant thickness of 8 mm was produced in a freezer completely attached to the DBD plasma actuator surface. After that, the actuator was tested in a cold ambient with a constant temperature of 15 °C. The deicing process was simultaneously monitored, by measuring the electrical signals, and visualized by using a high-resolution camera mounted above the DBD actuator. The camera used was *Orca R2 C1060010B* digital camera with a resolution of 1344 × 1024 pixels and the images were captured with a frame rate of 2FPS. A conventional light source was used to illuminate the actuator surface covered of ice in the interior of the “cold chamber”.

4. Results and discussion

4.1. Effect of dielectric material

The effect of dielectric material on the mechanical performance of DBD plasma actuators is reported in the literature [25]. However, the thermal and sensing performance of DBD plasma actuators with different dielectric material is not known. To investigate the effect of dielectric material on ice sensing and thermal performance of DBD

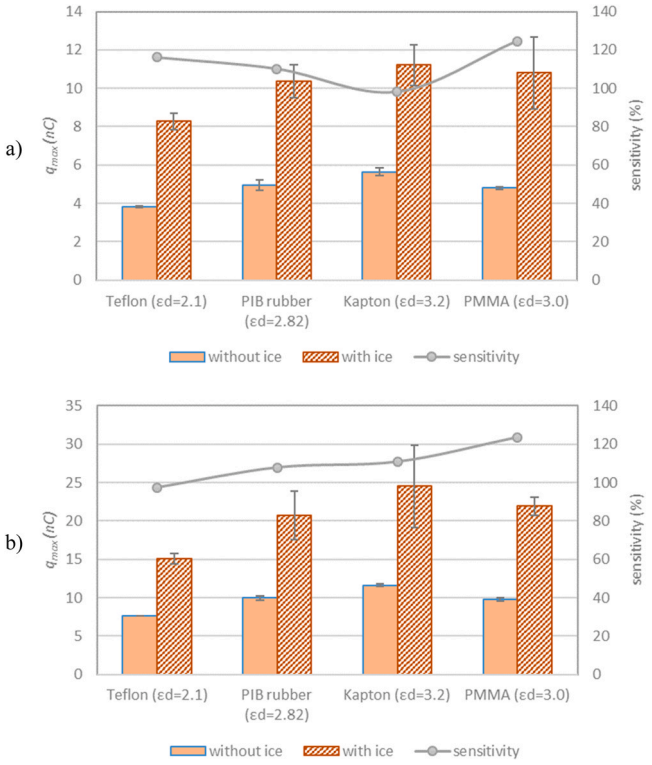

Fig. 6. Variation of the maximum charge measured by the monitoring capacitor for the DBD plasma actuators made by different dielectric material with/without the presence of ice cube for a) 2 kVpp b) 4 kVpp.

plasma actuators, four dielectric layers of Kapton, PMMA, PIB rubber and Teflon with 1 mm thickness were considered (Fig. 2). The relative dielectric permittivity for Kapton, PMMA, PIB rubber and Teflon at the ambient temperature and frequency of the applied voltage equal to 24 kHz is about 3.2, 3.0, 2.82 and 2.1, respectively. We should mention that these values may change during the experiments as the surface temperature and relative humidity (in the presence of ice) may vary. The area of all these dielectric layers was the same and equal to $5cm \times 8cm$, except for the PIB rubber where the area was smaller and equal to $4cm \times 8cm$. Although the area of PIB rubber was smaller, it did not limit the plasma discharge region and thus it did not have any influence on the plasma characteristics. In addition, the width of the exposed electrode and embedded electrode were 10 mm and 10 mm, respectively, and they were positioned asymmetrically without any gap ($l_g = 0mm$). These dimensions were used as reference values for studding the effect of dielectric material.

The contour plot of surface temperature for DBD plasma actuators that were fabricated using different dielectric materials, obtained by infrared measurements, are shown in Fig. 3. For all the dielectric materials, the highest temperature (hot spots) is produced at the edge of the exposed electrode and the heat is dissipated by conduction and convection. The heat convection is more obvious by the extension of isotherms further downstream, at the places located in the middle of the actuator. Those locations correspond to the points where highest ionic wind is produced. When PMMA is used the highest temperature is achieved, while the lowest temperature is obtained for Teflon.

The same trend is visible for lower voltages (7 kVpp) with the only difference being that the highest observed temperature is reduced (see Fig. 4). The reason that for the case of Teflon and PIB rubber that temperature is much smaller and non-uniform can be ascribed to the fact that the plasma ignition voltage for these materials is higher than PMMA and Kapton. Most of the heat dissipation for plasma actuators is related to the plasma formation and heat dissipation from the plasma region due to electron and ion Joule heating and also elastic and in-elastic collision between the electrons and ions exiting in the plasma cloud. When the DBD operates near to the ignition voltage, the density of charged species in the plasma region is very low and, in fact, plasma only appears as random weak sparks at some random points at the edge of the DBD plasma actuator. Therefore, in those cases, the measured temperature distribution is much lower and more non-uniform.

To grab a better idea about the strength and uniformity of thermal characteristics of the DBD actuators with different dielectric material, the maximum and average temperature of DBD plasma actuators over all the surface of the actuator and dielectric material are given in Table 1. The maximum and average temperature of the PMMA DBD was the highest and the Kapton DBD actuator resulted in the second highest maximum and average temperature. The high average temperature is a better merit when analyzing the thermal dissipation and its intensity. It can be seen that PMMA DBD actuator led to a more uniform temperature distribution due to less localized hot spots. In terms of durability of DBD actuator less hot spots can be an advantage, since many polymers such as Kapton may undergo rapid degradation when exposed to extremely high temperatures.

For an instantaneous detection of the presence of ice on the surface of the DBD plasma actuator, the voltage signals across the

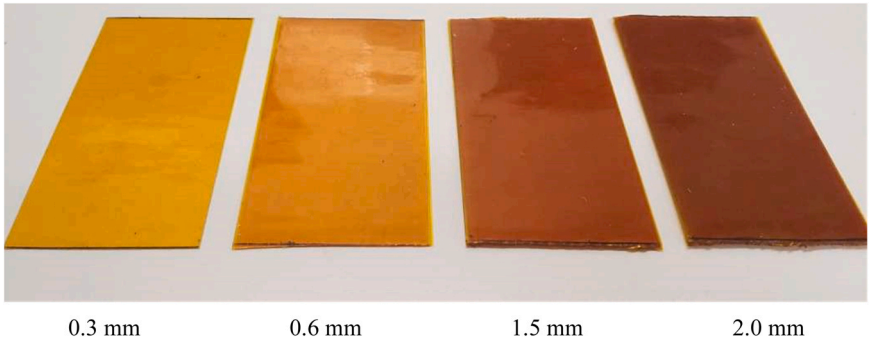

Fig. 7. Kapton dielectric layers with different thickness ranging from 0.3 to 2.0 mm.

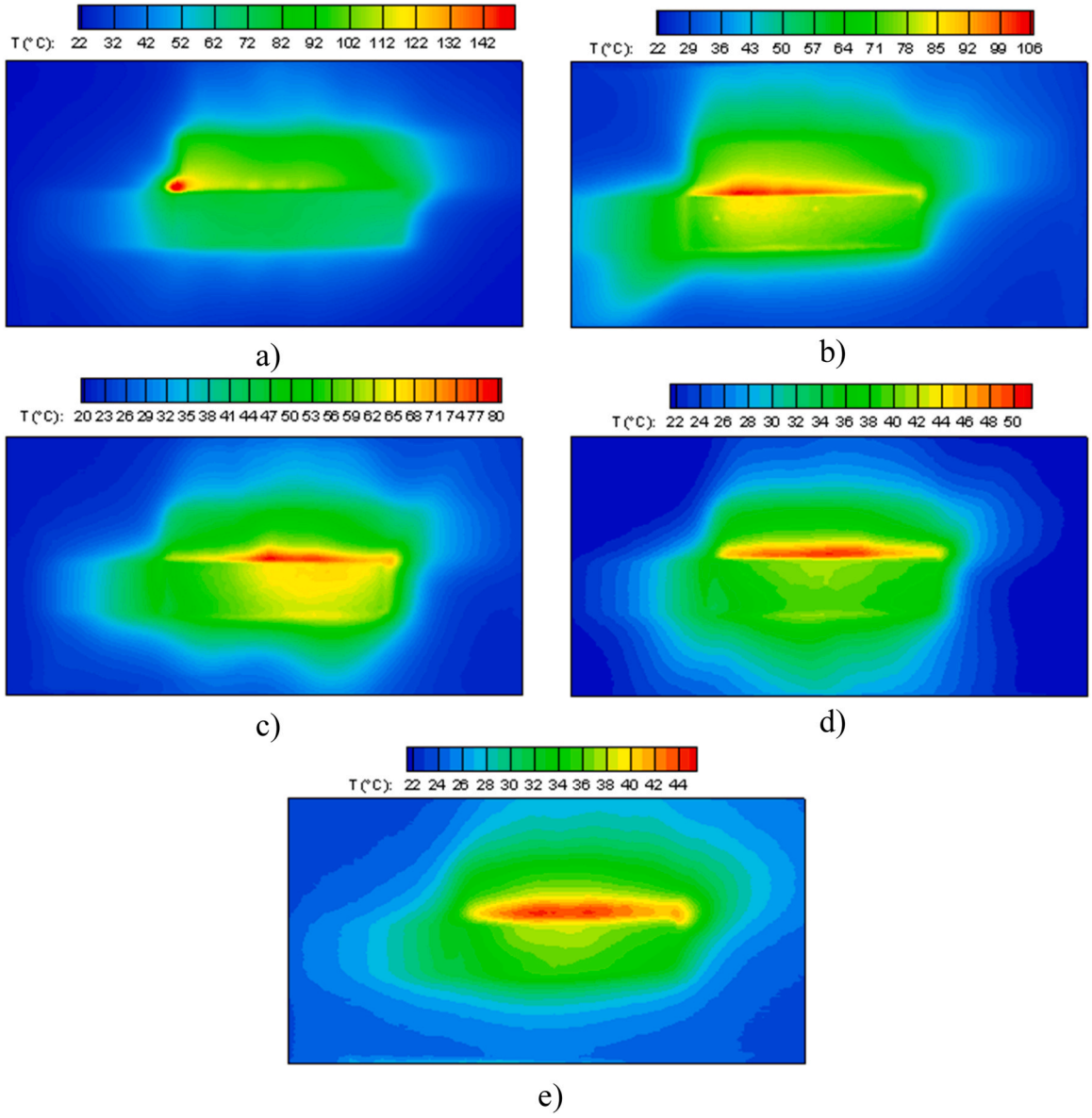

Fig. 8. Contour of surface temperature of the DBD plasma actuator operating at 8 kVpp for Kapton dielectric layer with thickness of a) 0.30 mm b) 0.60 mm c) 1.00 mm d) 1.50 mm and e) 2.04 mm.

Table 2
Maximum and average temperatures induced by the operation of the DBD plasma actuators with different dielectric material thickness.

Thickness	Operating voltage							
	5 kVpp		6 kVpp		7 kVpp		8 kVpp	
	T_{avg} (°C)	T_{max} (°C)	T_{avg} (°C)	T_{max} (°C)	T_{avg} (°C)	T_{max} (°C)	T_{avg} (°C)	T_{max} (°C)
0.30 mm	27.96	53.11	36.44	83.35	43.01	111.34	43.90	155.23
0.60 mm	27.04	36.75	30.64	53.90	36.42	79.20	45.22	104.43
1.00 mm	21.50	29.22	23.47	37.5	27.49	53.31	34.72	78.89
1.50 mm	20.38	24.14	21.62	31.08	24.28	39.35	28.16	50.17
2.04 mm	24.31	26.90	25.03	31.25	26.34	36.48	28.38	44.47

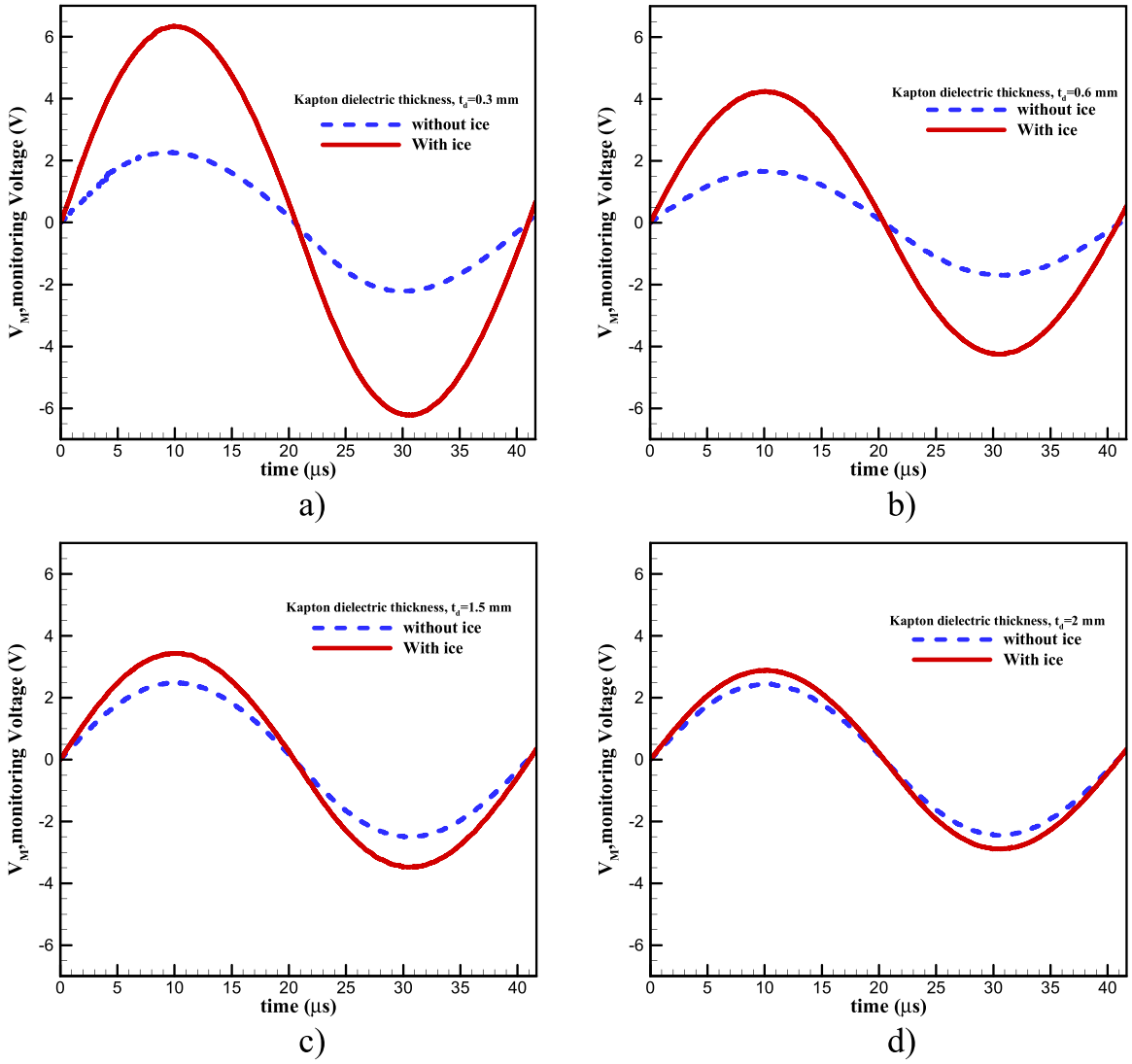

Fig. 9. Variation of the measured monitoring voltage at 4 kVpp and 24 kHz for the DBD plasma actuators with/without the presence of ice cube for Kapton dielectric layer with thickness of a) 0.30 mm b) 0.60 mm b) 1.50 mm and c) 2.04 mm.

sensing capacitor, which is placed in series with the actuator, were monitored and compared in the presence and absence of ice, and the corresponding results are given in Fig. 5. When an ice cube is placed on the DBD surface the voltage across the monitoring capacitor changes due to changes in capacitance of the actuator and ice system. For all cases, when the ice cube is placed over the surface of a given DBD, the corresponding voltage signal for that DBD increases significantly in magnitude ($V_{max} - V_{min}$).

For better analyzing the sensibility of the DBD actuators, the maximum charges q_{max}, measured by the use of the monitoring capacitor, are evaluated in the presence and absence of ice. In Fig. 6, the variation in the sensitivity of DBD plasma actuator with the change in the dielectric material is presented. The sensitivity is defined as the percentage of the variation of q_{max} in the presence of ice cube compared to the case without ice. The measurements of the ice sensing were conducted at two DBD operating voltages of 2 kVpp and 4 kVpp. When there is no ice cube on the DBD surface the measured values for the q_{max} show minimal error range, while in the presence of ice cube the measure range for q_{max} show higher dispersion. The results shown in Fig. 6, indicate the tested dielectric materials results in almost the same value for the ice sensitivity. However, Kapton DBD plasma actuator resulted in slightly lower sensitivity to presence of ice while PMMA DBD plasma actuator performed slightly better in terms of ice sensing. Some factors that could be the underlying reasons for the difference of the behavior can be different dielectric permittivity of the materials and layering methods for fabrication of the Kapton dielectric layer. The dielectric permittivity of Teflon, PIB rubber, PMMA and Kapton are 2.10, 2.82,

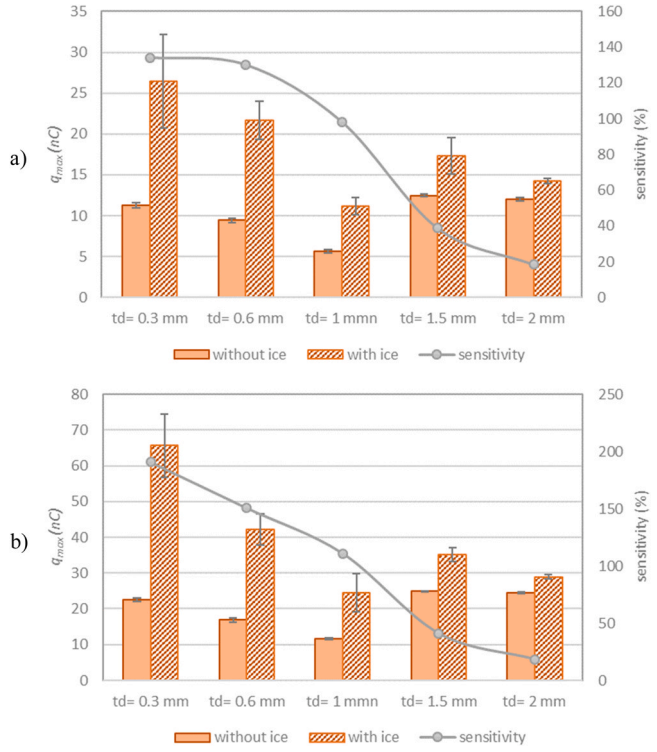

Fig. 10. Variation of the maximum charge measured for the DBD plasma actuators with different thickness of Kapton dielectric layers with/without ice for a) 2 kVpp and b) 4 kVpp.

3.00 and 3.20 respectively [26]. If we consider the dielectric permittivity of ice which is equal to 3.15, we can hypothesize that if the relative permittivity of dielectric material is close to the values of ice, the ice sensitivity of the actuator would be minimum. However, since the values of the dielectric permittivity of the materials that were tested were not that much different, and also considering that the values of the permittivity may change due to the variation in surface temperature and humidity, no clear conclusion can be taken about the effect of the dielectric permittivity on ice sensing.

4.2. Effect of dielectric thickness

To investigate the effect of dielectric thickness on sensing and thermal characteristics of DBD plasma actuators, five different Kapton layers with the respective thickness of 0.3 mm, 0.6 mm, 1.0 mm, 1.5 mm and 2.0 mm were fabricated by layering 5, 10, 17, 25 and 34 Kapton tape layers respectively (see Fig. 7). It should be mentioned that achieving dielectric thickness variation with other materials will be to some extent limited, since the minimum thickness of these materials available in our laboratory are relatively large and around 1 mm.

In Fig. 8, the contour plot of surface temperature of DBD plasma actuators with different thickness of dielectric layer is shown. For thinner dielectric layer at the same applied voltage, the surface temperature is significantly higher than those with thicker dielectric. To have a clear interoperation of this results, the driving mechanism for plasma formation which is the difference between the applied voltage and the ignition voltage must be considered. When the thickness of the dielectric layer is reduced the onset voltage (ignition voltage) is also reduced. Therefore, the difference of the applied voltage to the ignition voltage will be higher in case of thinner DBD plasma actuators and, thus, a stronger plasma region will form in case of thinner dielectric layers. It is obvious that stronger plasma region will exhibit a stronger thermal dissipation.

The higher surface temperature for thinner dielectric layers can be also observed at lower applied voltages. The higher achievable surface temperature with thinner dielectric layers may be nominating them as a better choice for deicing purpose. However, the problem of durability also must be considered at the same time. Higher surface induced temperatures may cause degradation of the dielectric material structure. The localized hot spots are evident of such change. Any degradation of the material or local hot spots put the material closer to its breakdown limit.

The maximum induced temperature and average surface temperature of DBD plasma actuator for different thickness of dielectric material are given in Table 2. The results in this table are indicating that there is a sharp drop in the maximum temperature (around 50 °C for 8 kVpp) when the dielectric thickness is increased from 0.3 mm to 0.6 mm. However, when the thickness of the dielectric layer is increased from 0.6 mm, the slop of drop in the maximum temperature becomes smaller, in a way that the drop of temperature is around 27 °C between 0.6.6 mm and 1.0 mm and 1.0–1.5 mm thickness for 8 kVpp. When the thickness of dielectric layer is increased more than 1.5 mm, the slope of the drop in surface temperature becomes smaller (around 6 °C between 1.5 mm and 2.0 mm for 8 kVpp). This trend in the behavior of maximum temperature is mostly related to the fact that for very low thickness of dielectric material, localized hot spots are the main reasons behind the high surface temperature. Also, for very thick dielectric material the applied voltage is much closer to the plasma ignition voltage which result in lower surface temperature.

The variation of the voltage signals across the sensing capacitor for the DBD plasma actuators with various thickness of Kapton dielectric material is given in Fig. 9. It should be noted that the result corresponding to dielectric thickness of 1 mm is given in Fig. 5c. The results indicate that for lower thickness of dielectric material the voltage across the monitoring capacitor is significantly increased when ice is present on the surface and for thicker dielectric material this voltage signal is less affected in the presence of ice.

The sensitivity of the DBD plasma actuators with different thickness of Kapton dielectric layer are shown in Fig. 10. The highest value of the charge measured by the DBD plasma actuator in the presence of ice was registered for the Kapton dielectric layer with the thickness of 0.3 mm. With the increase in the dielectric thickness the form 0.3–1.0 mm the stored charged in the DBD actuators system is reduced. When the dielectric layer is thin as 0.3 mm, the electric field is much stronger compared to the other cases and the higher charge formation due to ionization of air beside the DBD and higher ionic drifts accumulates more charges for thinner DBDs. To get an idea, the values of the ignition voltages can be considered for different DBD actuators. The ignition voltage of the 0.3 mm thin actuator is about 2.2 kVpp while the ignition voltage of 2.0 mm thick DBD actuator is about 6.5 kVpp. It is clear that when the operating voltage is higher than the ignition voltage the plasma formation is enhanced. Thus, in the presence of ice, the thinner DBD actuators will be affected more significant that the thicker ones due to

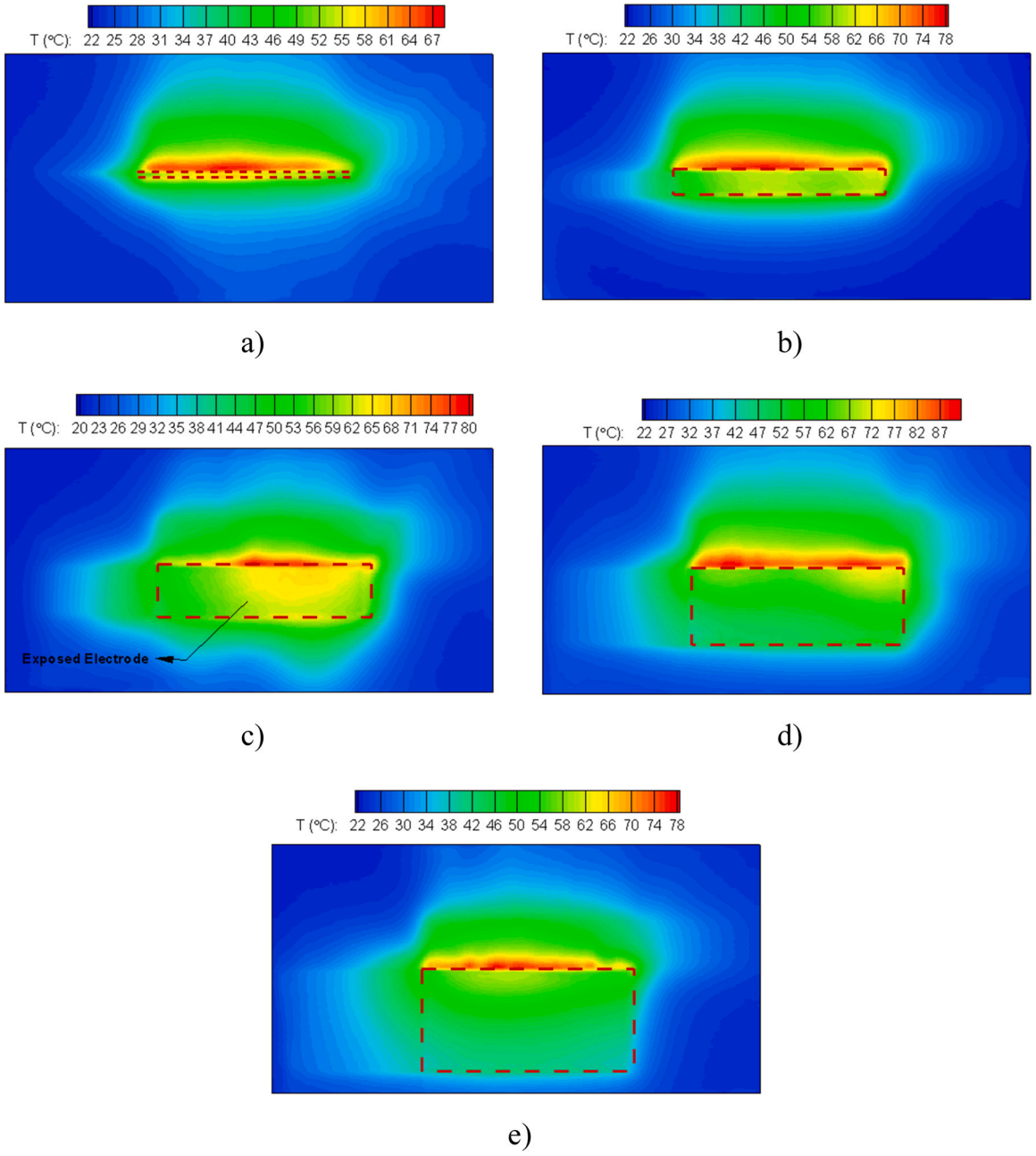

Fig. 11. Contour of surface temperature of the DBD plasma actuator operating at 8kVpp for exposed electrode with width of a) 1 mm b) 5 mm c) 10 mm d) 15 mm and e) 20 mm.

Table 3
Maximum and average temperature induced by the operation of the DBD plasma actuators with different width of exposed electrode.

l_{ex}	Operating voltage							
	5 kVpp		6 kVpp		7 kVpp		8 kVpp	
	T_{avg}(°C)	T_{max}(°C)	T_{avg}(°C)	T_{max}(°C)	T_{avg}(°C)	T_{max}(°C)	T_{avg}(°C)	T_{max}(°C)
1 mm	23.19	28.24	24.31	37.79	26.90	49.71	30.67	67.19
5 mm	21.85	28.02	23.63	39.25	26.87	50.35	32.58	77.16
10 mm	21.50	29.22	23.47	37.50	27.49	53.31	34.72	78.89
15 mm	23.97	27.85	26.24	43.15	31.68	60.93	39.91	90.39
20 mm	23.55	31.45	27.03	40.13	30.35	53.63	35.18	77.36

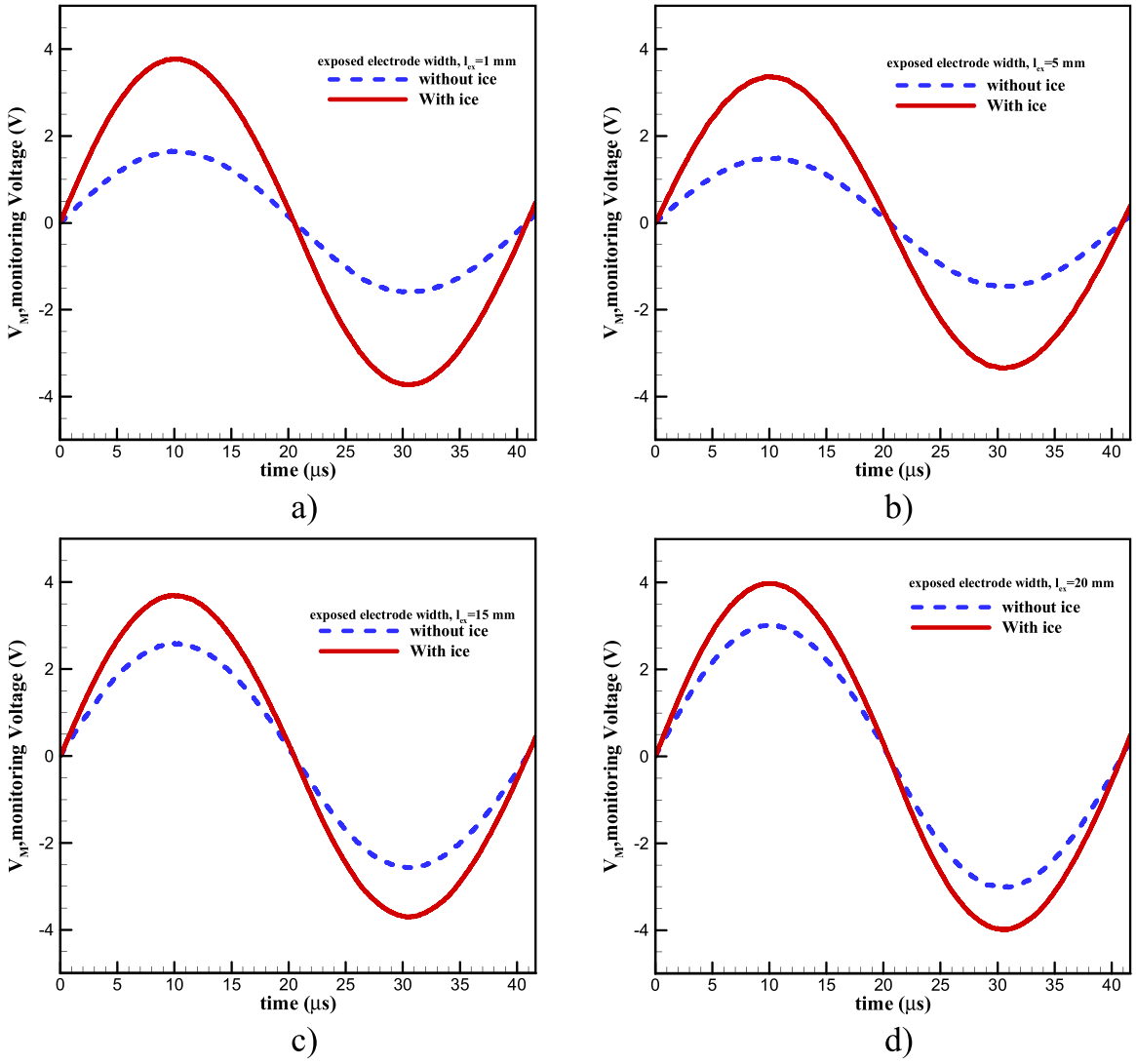

Fig. 12. Variation of the measured monitoring voltage at 4 kVpp and 24 kHz for the DBD plasma actuators with/without the presence of ice cube for exposed electrode with the width of a) 1 mm b) 5 mm b) 15 mm and c) 20 mm.

stronger electric field, and as a result, thinner DBD actuators will have better ice sensitivity. We can conclude from the results that with the increase in the thickness of the DBD the sensitivity is reduced.

Although DBD plasma actuators with thinner dielectric layers had shown to have better heating and ice sensing performance, considering them as ice sensor and deicing systems should be done cautiously because of rapid degradation. Generally, the durability of the thinner DBDs is much less than thicker DBDs due to degradation of the material because of exposure to high temperature and electric fields. In addition, operating the thinner DBD plasma actuators with higher operating voltages may not be possible because of the electrical breakdown of thin dielectric material at high voltages.

4.3. Effect of the width of exposed electrode

To study the influence of exposed electrode width on the thermal and ice sensing characteristics of DBD plasma actuators, five DBDs with exposed electrode width from 1 mm to 20 mm were fabricated and tested. The contour plots of surface temperature for varying exposed electrode width are shown in Fig. 11. One very clear observation in these figures is that, when the width of exposed

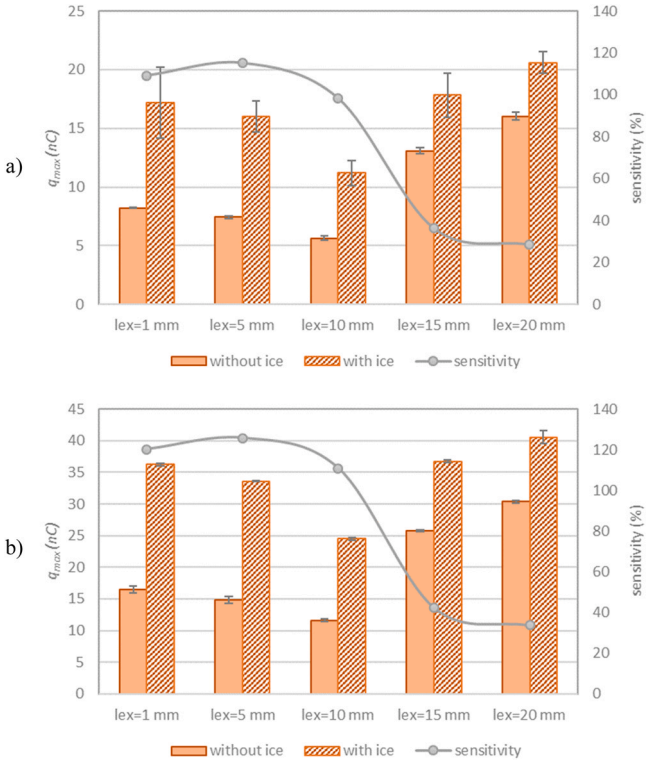

Fig. 13. Variation in the maximum charge for the DBD plasma actuators with different width of exposed electrode for the case with/without ice a) 2 kVpp and b) 4 kVpp.

electrode is increased, the surface temperature is dissipated more upstream the flow direction. This is related to surface conductivity of copper electrode which allows more conduction of heat to downstream locations.

In Table 3, the maximum and average surface temperature of the DBD plasma actuator with different width of exposed electrode for various operating voltage are reported. When the exposed electrode width is increased from 1 mm to 15 mm, the maximum surface temperature is increased and then when the exposed electrode width is increased more than 15 mm, the surface temperature is decreased. The maximum surface temperature occurs when the width of the exposed electrode is equal to 15 mm. In terms of maximum temperature, the 15 mm exposed electrode at 8 kVpp has 11 °C higher temperature compared to the second highest temperature for 10 mm width exposed electrode and in terms of average surface temperature, it has 5 °C higher temperature. The reason for higher surface temperature at exposed electrode width of 15 mm is that the ionization strength depends on the magnitude of the electric field. When the width of exposed electrode is changed the electric potential will be altered and consequently the intensity of the plasma region and the resulting thermal dissipation will change [27].

The variation of the voltage signals across the sensing capacitor for the DBD plasma actuators with various width of exposed electrode is given in Fig. 12. It should be mentioned that the results corresponding to exposed electrode width of 10 mm are given in Fig. 5c. The results show that when the width of the exposed electrode is changed, the voltage signal of sensing capacitor with/without the presence of the ice is affected. However, for smaller width of the exposed electrode the amplitude of the voltage signal in the presence of ice is increased more compared to the cases with larger width of the exposed electrode.

In Fig. 13, the maximum charge measured by the monitoring capacitor is compared for the case with and without ice for different width of the exposed electrode. The results indicate that when the electrode has a width less than 10 mm the charge with/without ice reduces with the increase in the width of the exposed electrode. However, when the exposed electrodes are wider than 10 mm, the charge on the surface both for the cases of with and without ice increases gradually. These trends in the maximum charge measured for different width of the exposed electrode, resulted in the ice sensitivity which has the largest values for the exposed electrode width lower or equal to 10 mm and the minimum ice sensitivity for the DBDs with the exposed electrode width larger than 10 mm.

4.4. Effect of width of embedded electrode

The influence of the embedded electrode width on the thermal and ice sensing characteristics of DBD plasma actuators are reported in this section. All the other parameters of the DBD actuators are equal to the reference case except the width of the embedded electrode which is varied from 1 to 20 mm. Fig. 14 shows the contour plots of the surface temperature of the DBD plasma actuator for various size of the embedded electrodes. An obvious effect of the width of the embedded electrode is that wider embedded electrode allows a better development and larger extension of the plasma region on the surface. When the embedded electrode is thin the plasma region is confined in a narrow region. For wider electrodes, plasma region is more extended and, thus, the thermal dissipation is occurring on a larger surface. However, the variation in the surface temperature between different cases are very small and if one considers the maximum and average temperature for all the operating voltages, it can be concluded that the effect of embedded electrode width on the surface temperature of the DBD is insignificant.

The average temperature and the maximum temperature of the DBD plasma surface area with different width of embedded electrode is given in Table 4. The results in this table shows that the influence of the width of the embedded electrode on the surface temperature is not significant. However, one observable trend in the values of the average and maximum surface temperature, suggest that with the increase in the width of the embedded electrode there is a slight increase in the surface temperature which can be related to better extension of the plasma discharge region.

Fig. 15 shows the variation of the voltage signals across the sensing capacitor for the DBD plasma actuators with various width of embedded electrode. The results corresponding to embedded

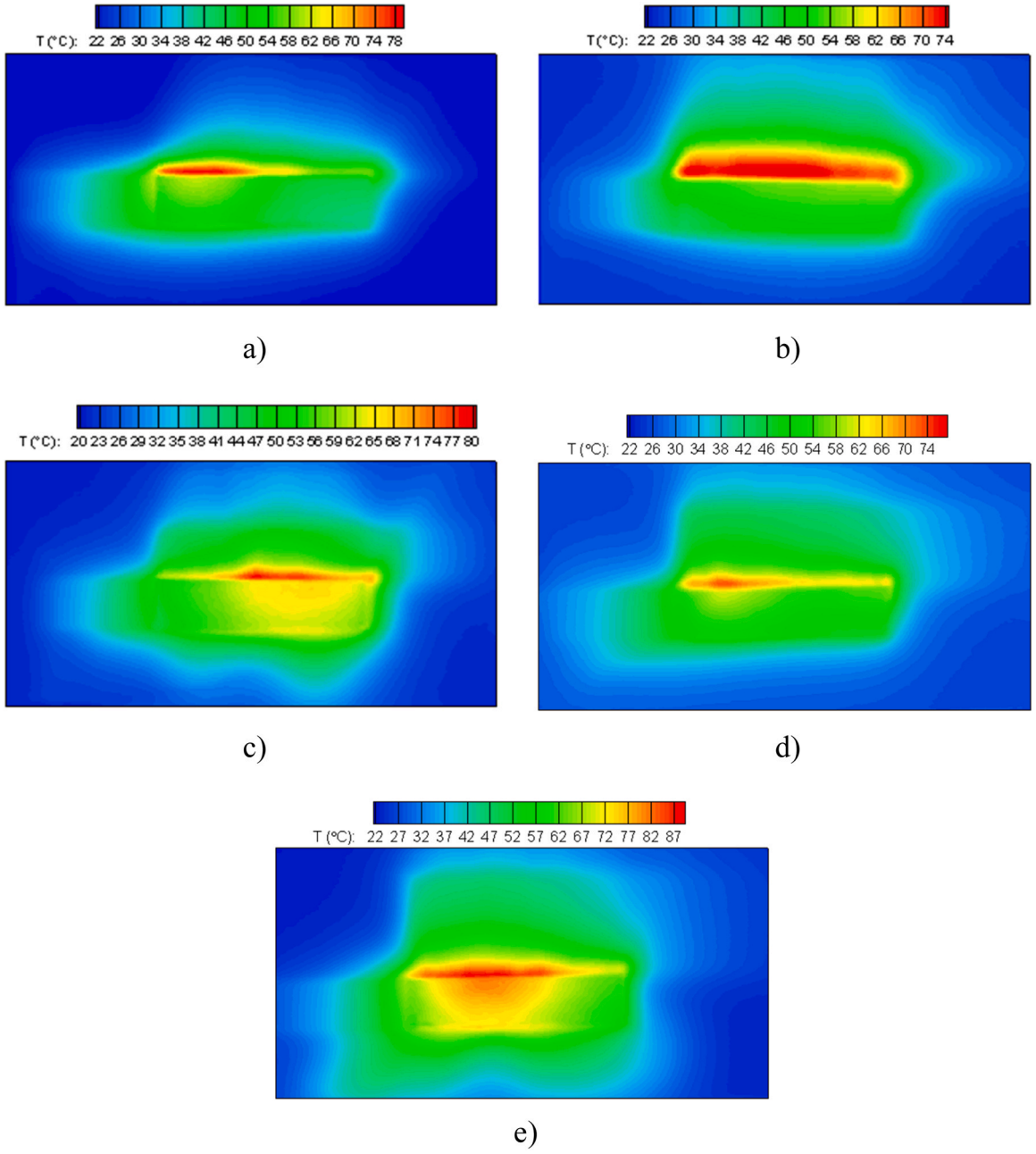

Fig. 14. Contour of surface temperature of the DBD plasma actuator operating at 8kVpp for embedded electrode with width of a) 1 mm b) 5 mm c) 10 mm d) 15 mm and e) 20 mm.

Table 4
Maximum and average temperature induced by the operation of the DBD plasma actuators with different width of embedded electrode.

l_{em}	Operating voltage							
	5 kVpp		6 kVpp		7 kVpp		8 kVpp	
	T_{avg} (°C)	T_{max} (°C)	T_{avg} (°C)	T_{max} (°C)	T_{avg} (°C)	T_{max} (°C)	T_{avg} (°C)	T_{max} (°C)
1 mm	19.38	25.66	21.97	40.98	25.80	58.94	30.37	78.31
5 mm	23.68	27.8	25.79	38.95	29.24	50.50	34.95	76.33
10 mm	21.50	29.22	23.47	37.50	27.49	53.31	34.72	78.89
15 mm	25.92	29.66	27.48	39.46	31.13	51.52	35.76	73.17
20 mm	23.37	28.28	25.87	40.53	28.87	51.27	41.67	88.86

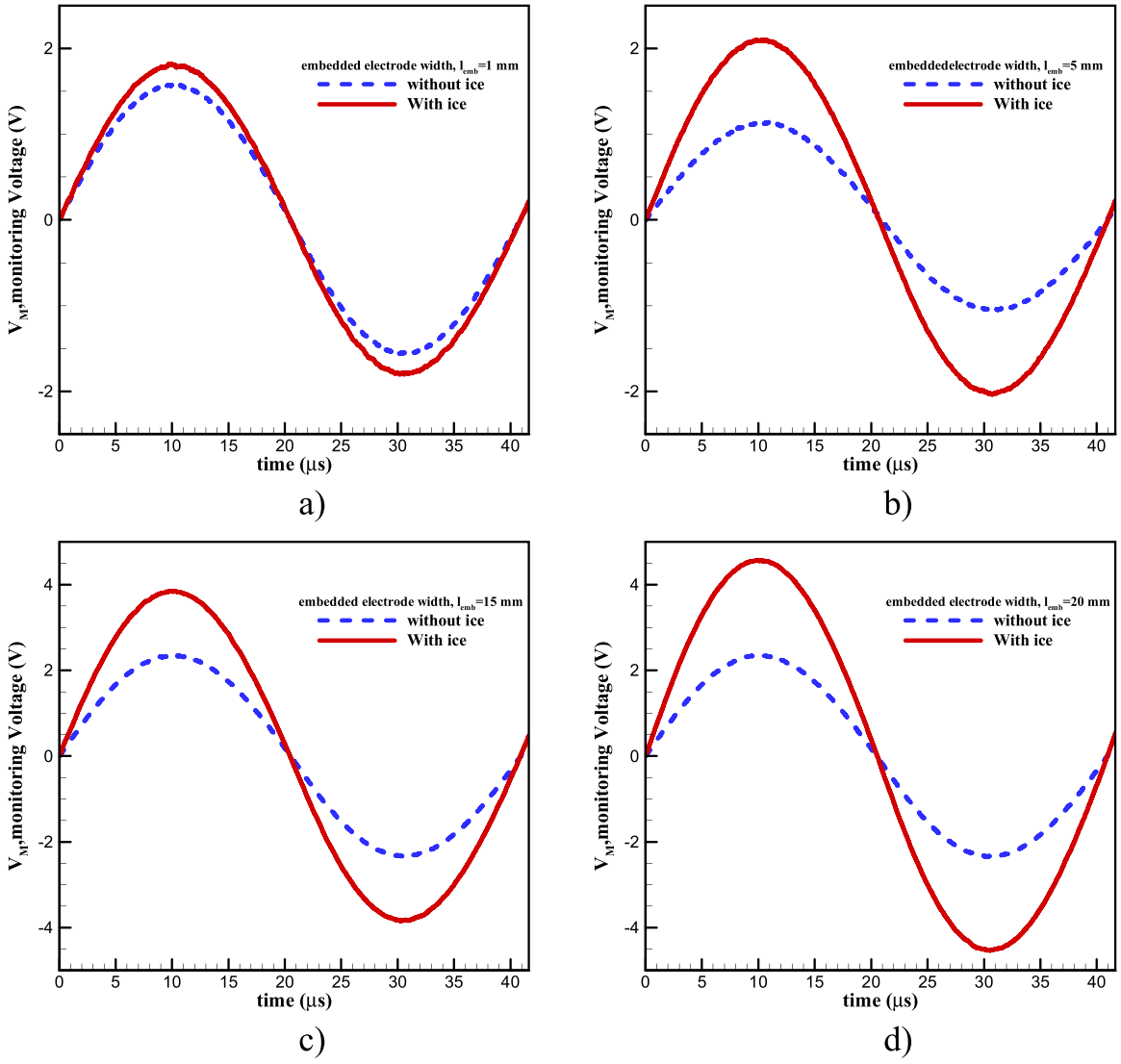

Fig. 15. Variation of the measured monitoring voltage at 4 kVpp and 24 kHz for the DBD plasma actuators with/without the presence of ice cube for embedded electrode with the width of a) 1 mm b) 5 mm b) 15 mm and c) 20 mm.

electrode width of 10 mm are given in Fig. 5c. The results show that for very low width of embedded electrode the voltage signal of the sensing actuator is changed very slightly in the presence of ice. However, for the larger width of the embedded electrode the change in the voltage signal due to presence of ice is more significant.

In Fig. 16, the sensitivity and the maximum charge measured for the DBD actuators in the presence of ice and without ice are reported for two working voltages of 2 kVpp and 4 kVpp. Wider embedded electrode in principle will lead to higher storing of the charge on the surface. In fact, the DBD system can be assumed as a capacitor. Larger area of the capacitor (imposed by wider exposed electrodes) is the reason that measured charge values for the cases with/without ice increase with increase in the width of the embedded electrode. In addition, larger embedded electrodes in general should be more sensitive to the presence of ice since a larger area of their discharge surface will be affected by the presence of ice. However, when the width of the embedded electrode is increased the electric field intensity probably will be change in a way that variation of the electric fields due to presence of ice is reduced. In Fig. 16a, when the voltage is 2 kVpp, the initial increase in the width of embedded electrode leaded to better ice sensing. However, the further increase of the embedded electrode width resulted in reduction of the ice sensitivity which was followed by almost a plateau for even wider embedded electrode. For 2 kVpp, the electric field strength is quite weak and possibly from 10 mm exposed electrode due to a wider diffusion area of the electric potential lines, the sensing performance will drop. However, for higher voltage of 4 kVpp, the sensitivity is increased with the increase in the width of embedded electrode. In

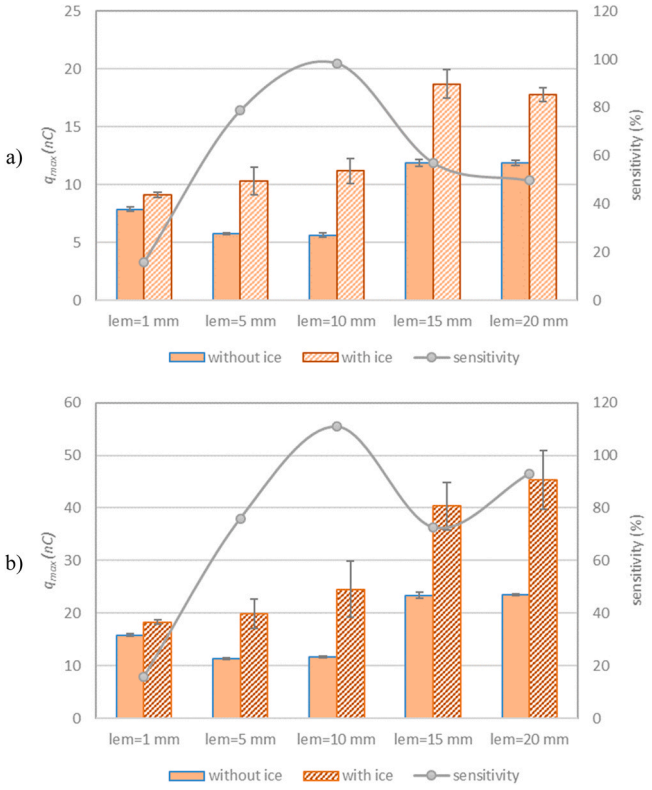

Fig. 16. Maximum charge and ice sensitivity measured for the DBD plasma actuators with different width of embedded electrodes for the case with/without ice a) 2 kVpp and b) 4 kVpp.

fact, two factors of higher surface charge due to larger surface area and electric field strength influence the sensitivity of the DBD. At 4 kVpp, when the embedded electrode width is larger than 10 mm, the increase in the surface area is aiding the sensitivity and the electric field is reducing the sensitivity.

4.5. Effect of width of gap between electrodes

The effect of axisymmetric gap (l_g) between the exposed and embedded electrodes on the sensing and thermal properties of DBD plasma actuator is studied in this section. We have tested 2 mm overlap of electrodes (negative gap) and also spacing between electrodes (positive gap) from 0 mm to 6 mm. Previous experiments had shown that there is an optimum gap spacing that would result in the best mechanical performance (induced flow) of DBD plasma actuator [28,29]. Therefore, in principle, an optimum gap spacing could exist for ice sensing and thermal performance of the DBD. Contour plots of the surface temperature of the DBD plasma actuator with different gap spacing are given in Fig. 17. As it can be seen the highest surface temperature is measured when the gap length is between − 2–2 mm. Any further increase in the gap length will result in sharp reduction of the surface temperature. This behavior can be explained in terms of the electric field strength and the dependency of the plasma formation on the electric field. Excessive increase in the gap length will result in reduction of electric field strength that is needed to produce the plasma. However, when an optimum value of gap length is selected the electric field is sufficient to maintain a uniform and stable plasma region which is extended further on the surface.

The average temperature and the maximum temperature of the DBD plasma surface area with different gap length are given in Table 5. The maximum temperature shows the highest temperature that locally was generated. This temperature in some case may show the temperature of hot spots that are created when strong streamers are formed. The average temperature shows however the uniformity of the thermal dissipation on the surface area of the DBD. When the average temperature is closer to the maximum temperature and also the average temperature is the maximum, it can be concluded that the thermal performance is the best. At 8 kVpp, the maximum surface temperature over 80 ℃ was recorded for a DBD with 2 mm gap. However, at this operating voltage the highest average surface temperature was resulted for the case with zero gap spacing (34.72 ℃). For lower operating voltages, the negative overlap of the electrodes, leads to a higher maximum and average surface temperature. The gap length defines the extend of the plasma regions and also defines the magnitude of the effective electric field for plasma formation. It is obvious that lower spacing or negative overlap of the electrodes help to achieve higher plasma formation while increase in the spacing will allow better extension of the plasma region. For a negative overlap at 8 kVpp, the plasma region is forced to be concentrated on a smaller region and thus the surface temperature is lower compared with the case with zero spacing. However, for lower operating voltage, the negative overlap is sufficient for the extension of the plasma and also the electric field strength is higher and as a result the surface temperature is slightly higher than the zero gap actuator.

Fig. 18 shows the variation of the voltage signals across the sensing capacitor for the DBD plasma actuators with various width of asymmetric gap between the exposed and embedded electrodes. The results corresponding to the actuator with no gap are given in Fig. 5c. The results show that for the negative overlap of the electrodes (−2 mm gap), the voltage signal in the presence of ice is less increased in comparison to the positive gap lengths. For the positive gap length, further increase of the gap length from 2 mm does not change the relative amplitude of the voltage signal in the presence of ice compared to the case without ice $((V_{max} - V_{min})_{without} - (V_{max} - V_{min})_{with})$.

The sensing capability of DBD plasma actuators with different gap length between electrodes was examined and the results are given in Fig. 19. The results indicate that the value of charge measured by the monitoring capacitor is maximum when the gap length is negative. Moreover, the measured value of charge also decreases sharply with the increase of the gap length from 0 mm to 6 mm. When an ice cube is placed on the DBD, the values of the charge experience a sharp increase for all the cases. The variation of ratio of

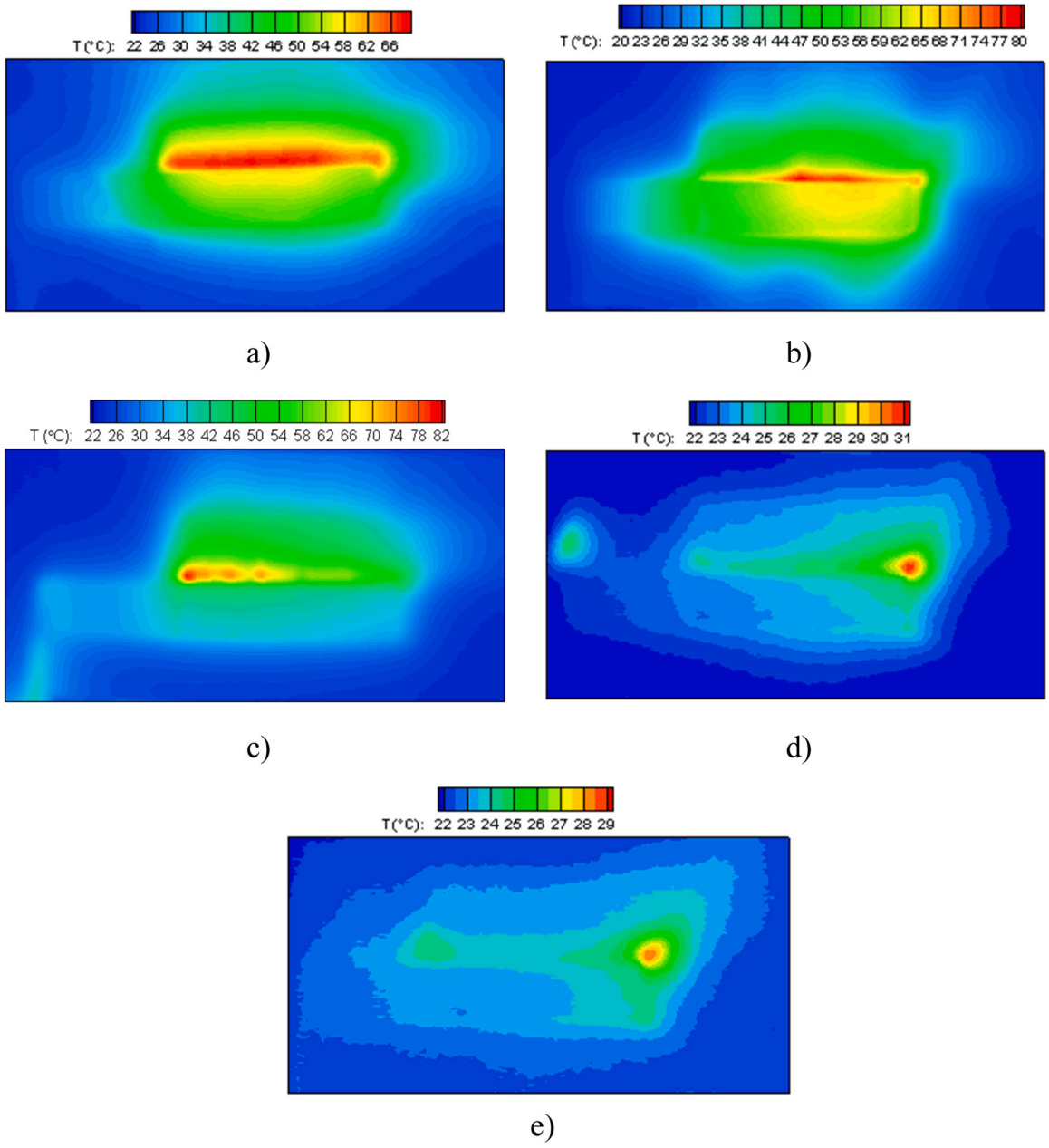

Fig. 17. Contour of surface temperature of the DBD plasma actuator operating at 8 kVpp for gap spacing of a) − 2 mm b) 0 mm c) 2 mm d) 4 mm and e) 6 mm.

Table 5
Maximum and average temperature induced by the operation of the DBD plasma actuators with different width of gap length.

l_g	Operating voltage							
	5 kVpp		6 kVpp		7 kVpp		8 kVpp	
	T_{avg} (°C)	T_{max} (°C)	T_{avg} (°C)	T_{max} (°C)	T_{avg} (°C)	T_{max} (°C)	T_{avg} (°C)	T_{max} (°C)
-2 mm	25.38	34.05	27.68	48.75	29.82	52.42	34.52	68.41
0 mm	21.50	29.22	23.47	37.50	27.49	53.31	34.72	78.89
2 mm	22.44	27.06	23.81	30.45	26.12	39.93	32.81	80.30
4 mm	21.54	22.77	22.85	26.68	23.27	28.96	22.73	30.91
6 mm	22.04	23.02	22.54	23.81	22.94	25.63	22.90	28.35

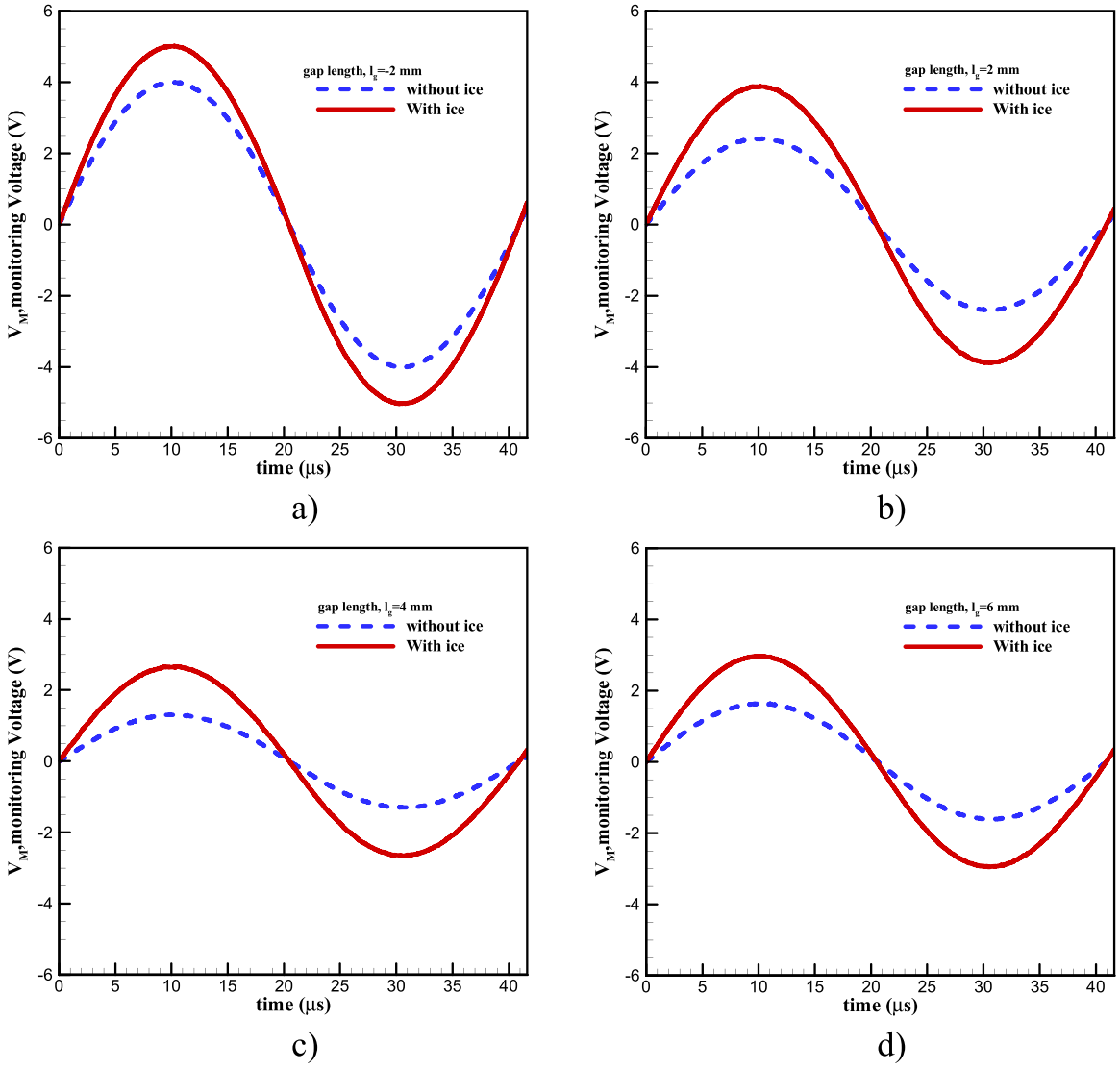

Fig. 18. Variation of the measured monitoring voltage at 4 kVpp and 24 kHz for the DBD plasma actuators with/without the presence of ice cube for the electrodes gap width of a) −2 mm b) 2 mm b) 4 mm and c) 6 mm.

the increase in the maximum charge due to the presence of ice on the actuator undergoes a nonlinear trend with the maximum sensitivity to the ice recorded for the case with the gap of 2 mm at 2 kVpp and for the case with 4 mm gap at 4 kVpp. In fact, here for the gap length, two factors of plasma extension and intensity of plasma formation play an important role. When the gap length is increased the ignition voltage for plasma formation is reduced and thus less charges are accumulated on the surface and the electric field near the DBD is weaker. However, when the gap length is increased, the surface area of DBD where ice formation can have influence the sensing would increase. At 2 kVpp, the operating voltage is low and after 2 mm gap, the electric field becomes weaker and thus the sensing ability drops. For 4 kVpp, the applied voltage is high enough for the DBD to take advantage of both a stronger electric field and also larger sensing area at 4 mm gap. Thus, it can be concluded that an optimum gap spacing exists for DBD actuator in terms of sensing.

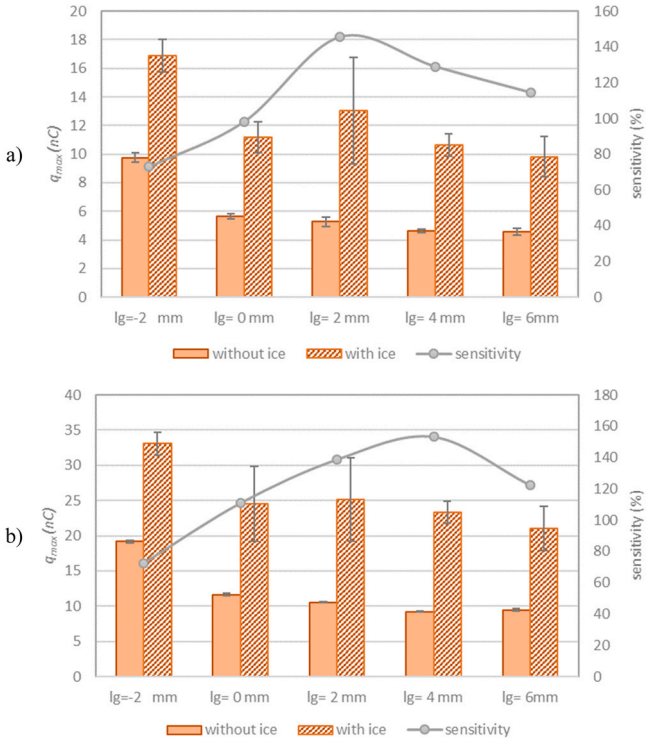

Fig. 19. Variation of the measured charged and ice sensitivity for the DBD plasma actuators with different gap length for a) 2 kVpp and b) 4 kVpp.

It is interesting to mention that when plasma actuators are used for flow control device, an optimum gap length also exist which leads to highest ionic wind.

4.6. Deicing test of DBD actuator with optimum dimension

According to the results shown in the previous section, we can rank the DBD plasma actuators according to their thermal and sensing behavior. In Table 6, the results of a ranked list of the DBD actuators are given. We should mention that some of the parameters that were studied had very low influence on the thermal and/or sensing behavior. For example, for the sensing, all of the dielectric material performed somehow similarly, for the embedded electrode the thermal behavior was not significantly influenced by the width of the electrode. From this table it is observed that the best thermal behavior of the DBD actuator can be achieved for an exposed electrode width of 15 mm, an embedded electrode width of 20 mm, a gap length of 0 mm, a dielectric thickness of 0.3 mm, and the dielectric material made of PMMA. In addition, the best parameters of the DBD actuator for ice sensing behavior is exposed electrode width of 5 mm, embedded electrode width of 5 mm, gap length of 2 mm, dielectric thickness of 0.3 mm, and the PMMA dielectric material. The only common parameters for the sensing and thermal characteristics are the dielectric material (PMMA) and the dielectric thickness (0.3 mm). Although PMMA was the material that showed the best overall behavior, the thickness available for it was limited to 1 mm and thus fabricating a DBD with 0.3 mm PMMA was not possible. On the other hand, if we compare the 1 mm PMMA actuator with the 0.3 mm Kapton actuator, clearly the Kapton actuator of 0.3 mm overcomes the PMMA of 1 mm in terms of both heating and sensing performance. Besides that, studies have also shown that thin plasma actuators allow to generate higher induced flow velocity [30]. Therefore, in order to access the performance of the DBD with optimum dimensions, we have built a DBD with Kapton with 0.3 mm thickness. For the other geometrical parameters, since reaching to an optimum set of data suitable for both thermal and sensing was not possible, we selected a 20 mm width embedded electrode, 5 mm exposed electrode and 0 gap for deicing test.

We have tested the above mentioned DBD actuator for its ability for simultaneous deicing and ice sensing. In order to reduce the effect of deicing due to heat transfer with surrounding, we have used an in-house built climate chamber which were able to maintain a constant temperature during the experiments at 15°C. The DBD actuator was tested at 4 kVpp and the variation of the charge seen by the monitoring capacitor and the evolution of the deicing process were recorded. During the ice melting process with DBD plasma actuator, when all the surface is covered with an ice layer with thickness of 8 mm, tracking the melting front is difficult. This is due to the controlled temperature of the chamber, which reduces the heat transfer between the ice and air. In Fig. 20, the evolution of the deicing process for the selected DBD is shown. The first visual variation of the ice layer was observed at around 135.5 s. At this moment a very small film of water was formed near the edges of electrodes. This water film then started to grow gradually into small drops where the layer was attached to cover all the surface of the actuator. At around 630 s, the ice layer above the large underneath drop started to melt and melting front on the surface appeared as a hole. With the progress of the deicing process this hole starts to widen and the surface deicing, near to the DBD surface progressed to right surface. After 1550 s a wide hole is observed, and the ice layer was detached from the surface. The deicing process can be

Table 6
Rank list of DBD plasma actuators dimensions based on their sensing and thermal characteristics.

	Thermal behavior					Sensing behavior				
	l_{ex} (mm)	l_{em} (mm)	l_g (mm)	*material*	t_d	l_{ex} (mm)	l_{em} (mm)	l_g (mm)	*material*	t_d (mm)
1	15	20	0	PMMA	0.3	5	10	2	PMMA	0.3
2	10	15	2	Kapton	0.6	1	5	4	Teflon	0.6
3	20	10	-2	PIB rubber	1	10	15	0	PIB rubber	1.5

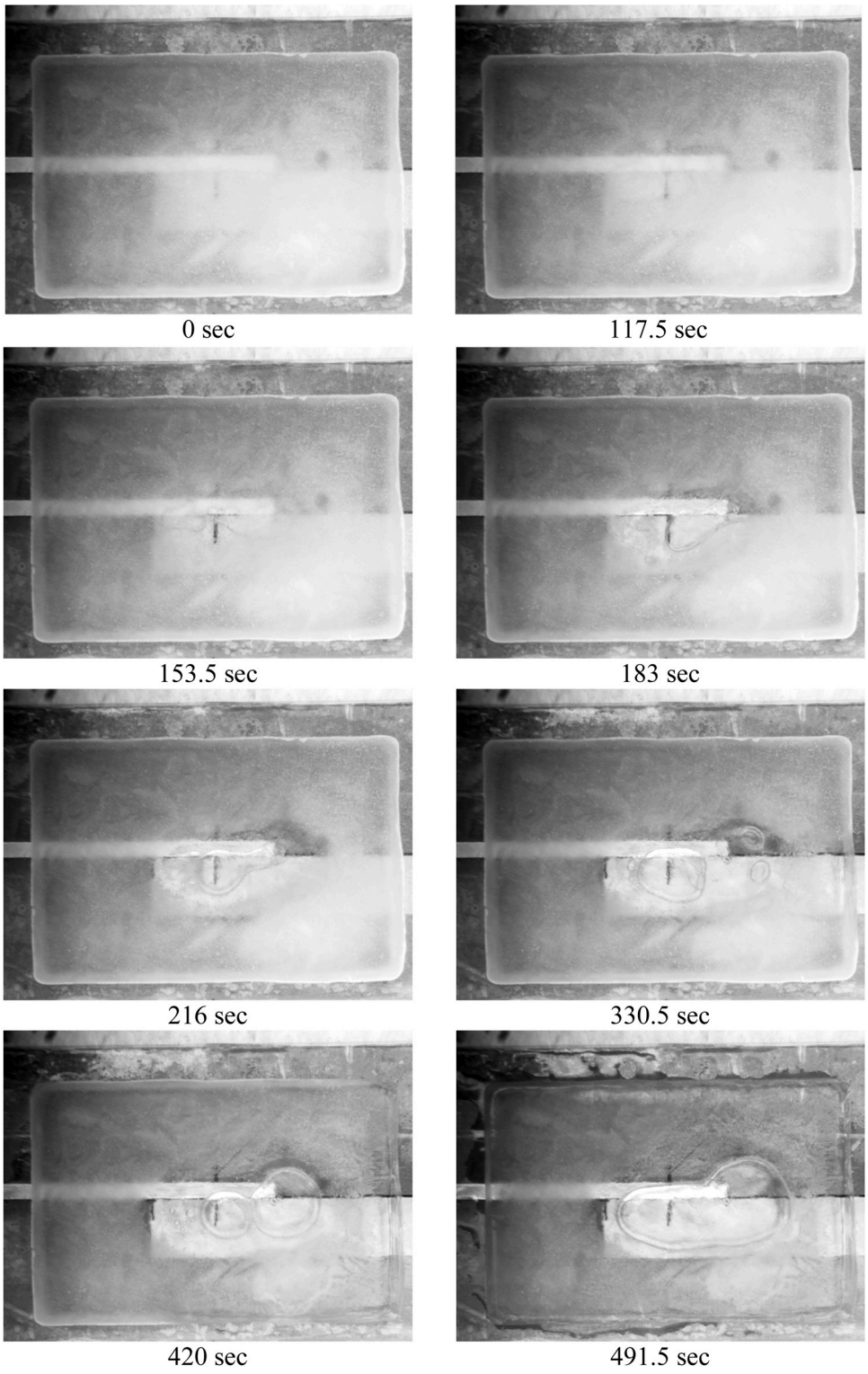

Fig. 20. Evolution of the deicing process of an 8 mm ice layer using DBD plasma actuator operating at 4 kVpp.

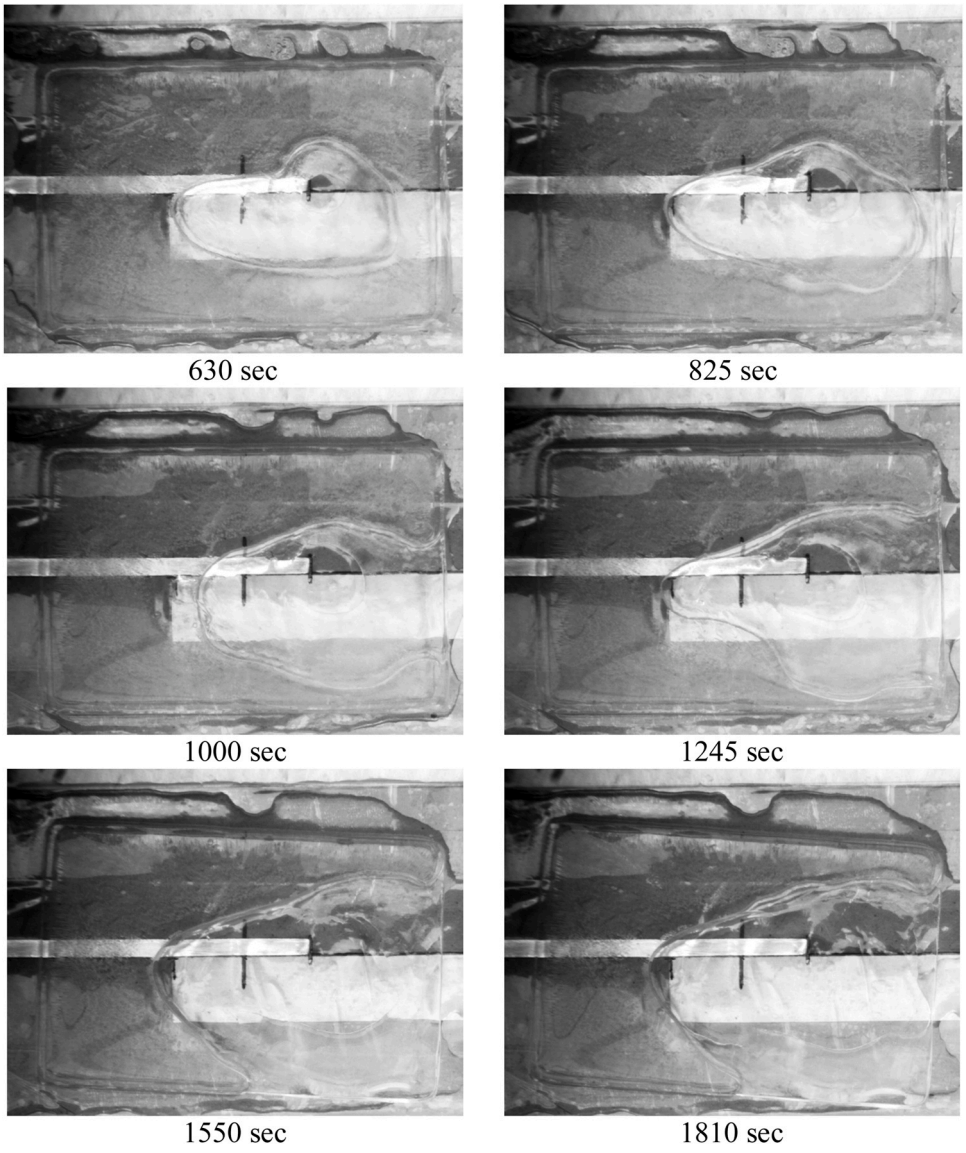

Fig. 20. (*continued*)

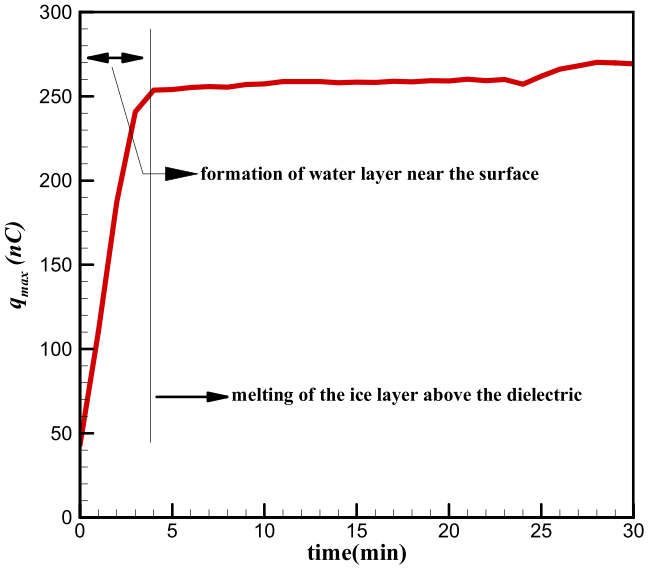

Fig. 21. Variation of the maximum charge measured by the monitoring capacitance during the deicing process of a 8 mm thick ice layer.

considered to have ended at this point. We should mention that the deicing process shown in Fig. 20 is slow and for aircraft icing, the anti-/deicing should be earlier and faster. The reason for the slow deicing process is related to the low power of the DBD actuator that was used. The power of the deicing process corresponding to the results of Fig. 20 were in the range of 0.2–7.66 Watt. Further increase in the deicing power by operating the DBD actuator at very high voltages was not possible since the power source (PVM500) was not enough potent to deliver the needed high power.

In Fig. 21, the variation of the maximum charge measured by the monitoring capacitor is given. The sharp variation in this figure is indicative of an event in the deicing process. The variation in maximum charge in this figure shows that from the start of the deicing process until 4 min, the maximum charge was increasing constantly. This increase in maximum charge values shows the accumulation and appearance of liquid water on the surface. After 4 min, the maximum charge stayed almost constant. This is an indication that all of ice that are in contact at the surface of the DBD already had been melted to thin water film. Since the surface is completely flat and this water does not drip out, we did not observe any more significant change on the maximum charge of the device.

To better demonstrate and also investigate the influence of the DBD actuator for deicing, soft frost was collected on a volume with the dimension of $6cm \times 10cm \times 1.7cm$ exactly on the surface of the DBD. Then the deicing behavior of the DBD was monitored and the plots of the deicing process are given in Fig. 22. The frost layer was melted almost completely around 13 min. The deicing process can be visually first observed about 70.5 s after the DBD plasma actuator starts its operation. The deicing was initiated mostly around the region on the surface of the exposed and embedded electrode mostly closer to the left side, where high voltage electrode was installed. The deicing then progressed from left side to right side, with tendency for higher melting rate on the surface of exposed electrode.

The variation of the maximum charge on the monitoring capacitor was recorded for the deicing process of the soft ice and are plotted in Fig. 23. Any sharp variation in the plot of q_{max} can be attributed to major events in the deicing process. Any reduction of the values of q_{max} signifies the reduction in the volume of the ice that covers the dielectric surface with minor or negligible water being present on the surface. Any increase in the values of the q_{max} means formation of interfacial water film or accumulation of the melted ice water on the surface. According to this figure the values of q_{max} until two minutes undergoes a slight reduction which means that the volume of the ice on the surface is reduced (it can be seen also in Fig. 16). Afterward, the q_{max} value starts to increase and fluctuate until 7 min with the values being above the initial value. During this time, major deicing process was on-going. Between 7 min to almost 11 min deicing was still progressing with water layer on the surface being far from the sensing zone. Afterwards, with formation and accumulation of large water films on the surface a sudden jump in the values of q_{max} is observed. This means that the majority of the soft ice has been melted and now the medium in contact with the surface of the DBD plasma actuator is mostly constituted by water.

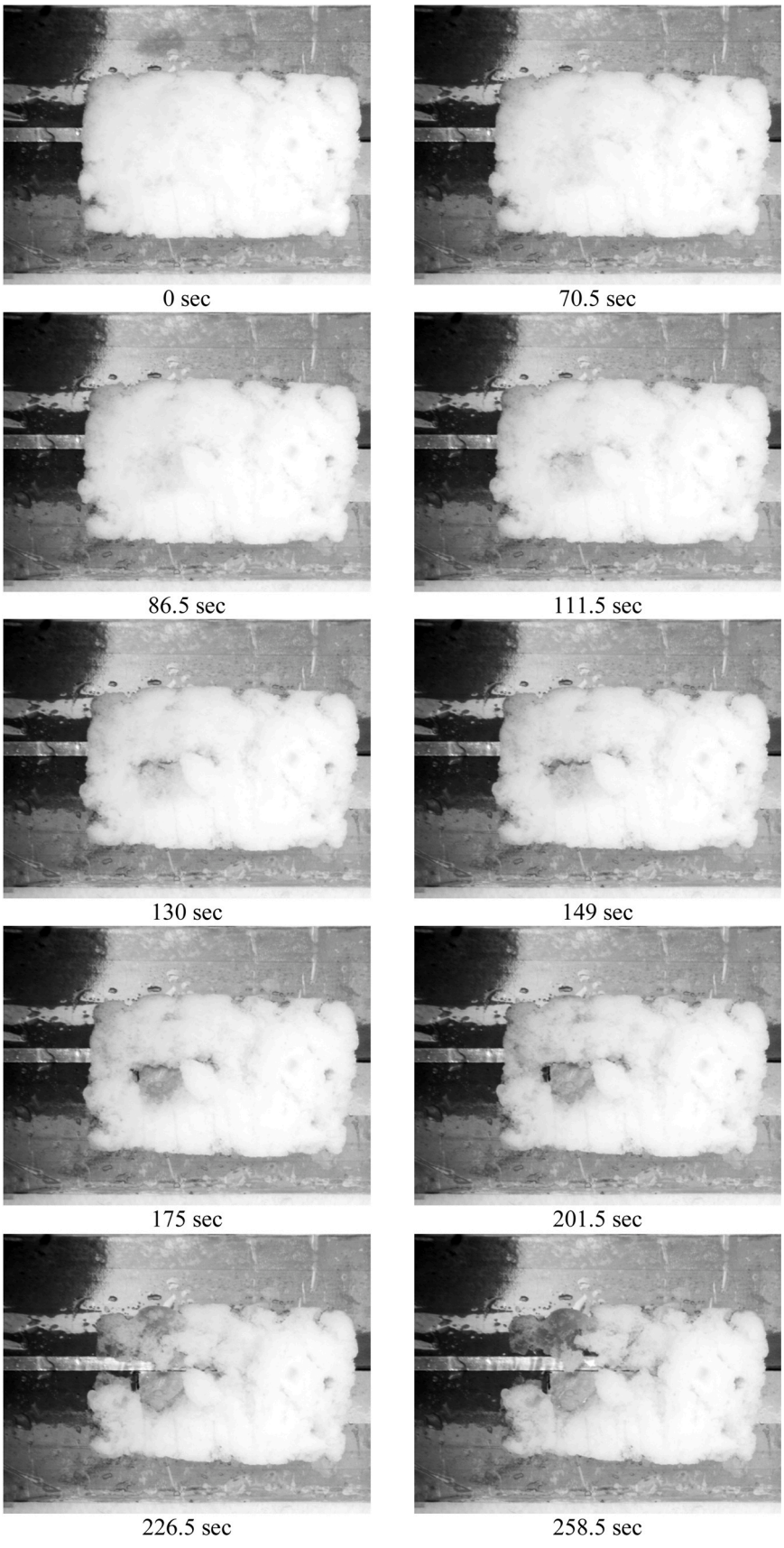

Fig. 22. Evolution of the dicing process of the soft ice with DBD plasma actuator operating at 4 kVpp.

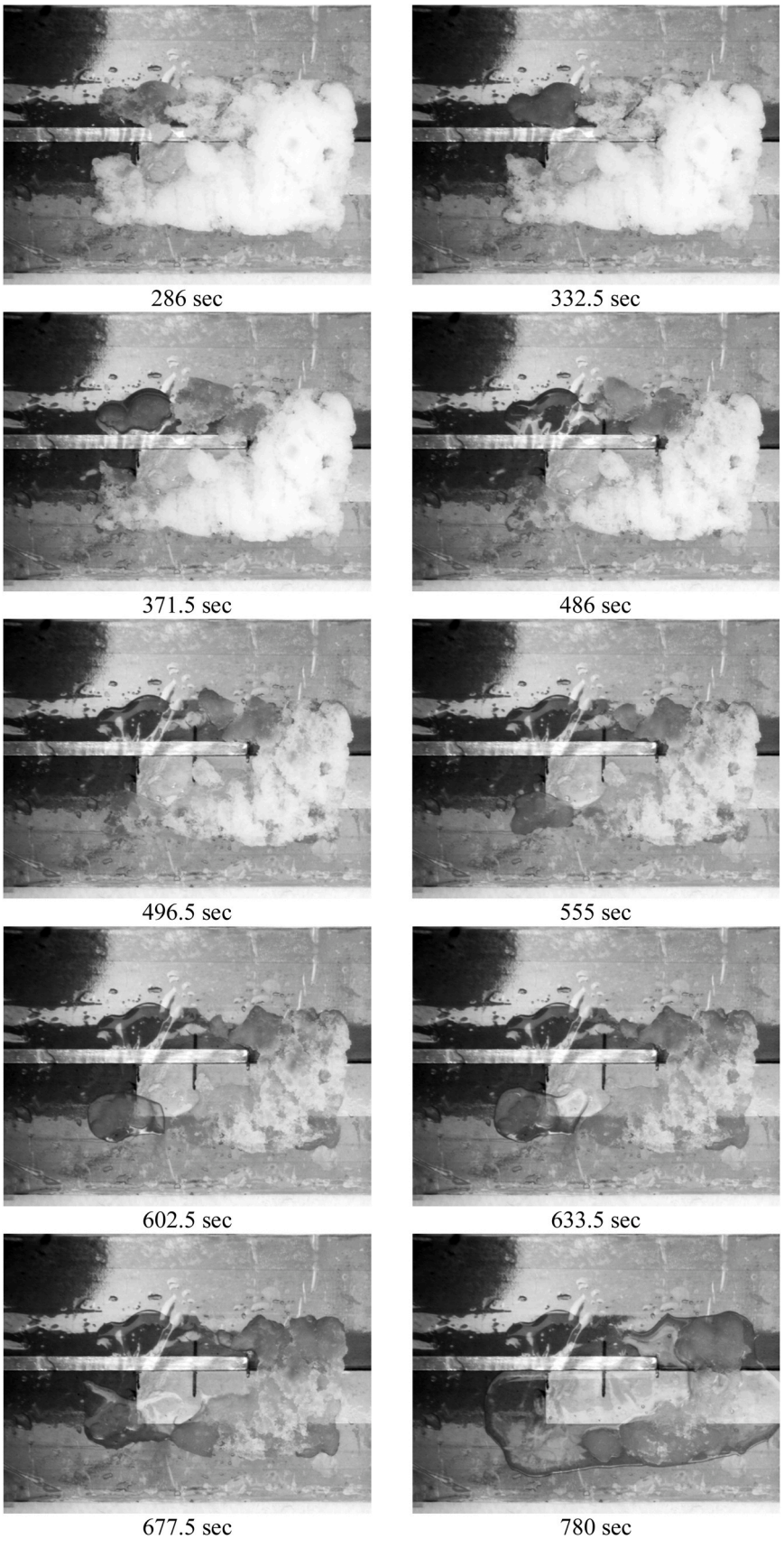

Fig. 22. (*continued*)

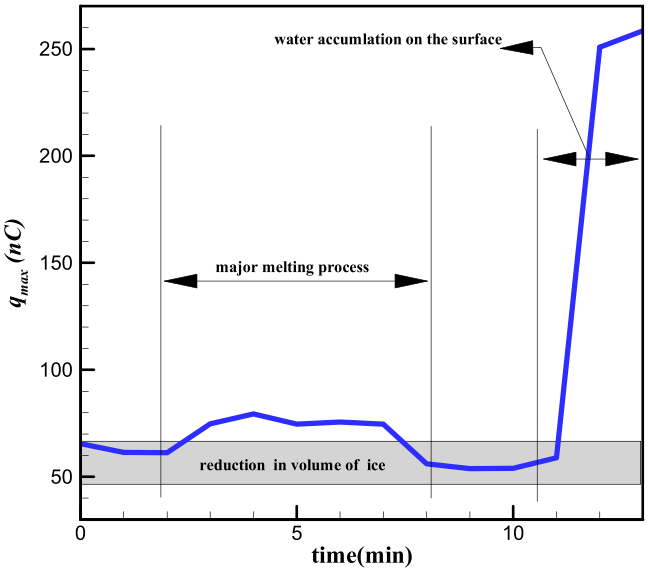

Fig. 23. Variation of the maximum charge measured by the monitoring capacitance for dynamic deicing of soft ice.

5. Conclusion

In this paper, an experimental parametric study is conducted in order to investigate influence of the main geometrical and physical parameters of DBD plasma actuator on thermal and ice sensing characteristics. The surface temperature of the DBD actuator were measured for various operating voltages ranging from 5 kVpp to 8 kVpp. The ice sensing capability of DBD actuator were evaluated by measuring the variation in maximum charge stored on the DBD with and without the presence of ice. In addition, the evolution of the deicing process for an ice layer and a layer of soft ice (frost) was presented. The main outcomes of this research are summarized as follows:

- The surface temperature of the DBD actuator depends on to the dielectric material. Among Teflon, PIB rubber, PMMA and Kapton, the highest surface temperature was obtained for PMMA and Kapton respectively. The ice sensitivity of the DBD various slightly with the change in the dielectric material of the DBD actuator.
- In terms of ice sensing and surface temperature, the thinnest dielectric material (0.3 mm) resulted in the best ice sensing and thermal characteristics.
- The maximum surface temperature of the DBD increased with the increase in the width of the exposed electrode from 1 mm to 15 mm and then it decreases with further increase in the width of the exposed electrode. In terms of ice sensing, the 5 mm exposed electrode resulted in the best ice sensing. The ice sensitivity of 1 mm and 10 mm width exposed electrode were slightly lower than the case with 5 mm exposed electrode. When the width of the exposed electrode was increased further from 15 mm, the ice sensitivity decreases sharply.
- The influence of the embedded electrode on the surface temperature of the DBD is low. However, there exist an optimum width of embedded electrode in terms of ice sensing.
- For axisymmetric gap length between the exposed and embedded electrode exists optimum value in terms of surface temperature and ice sensing. At 8 kVpp the surface temperature of the DBD with 2 mm gap was maximum. Ice sensing evaluation also showed that at 2 kVpp the 2 mm gap is the optimum while at 4 kVpp the 4 mm gap showed the best ice sensing.

CRediT authorship contribution statement

M. Abdollahzadeh: Conceptualization, Methodology, Visualization, Validation, Investigation, Writing – original draft preparation, Writing – review & editing, Funding acquisition. **F. Rodrigues**: Conceptualization, Methodology, Investigation, Data Curation, Writing – original draft preparation, Writing – review & editing. **J. Nunes-Pereira:** Conceptualization, Methodology, Investigation, Writing – original draft preparation, Writing – review & editing. **J.C. Pascoa**: Investigation. Writing – review & editing, Funding acquisition, Resources. **L. Pires:** Writing – review & editing, Resources.

Declaration of Competing Interest

The authors declare that they have no known competing financial interests or personal relationships that could have appeared to influence the work reported in this paper.

Acknowledgments

The research work was supported by FCT Project CEECIND/03347/2017 (Smart blade based on printed sliding dielectric barrier discharge plasma actuators and higher harmonic motion for ice removal of cycloidal wind turbine), while parts of the work were supported by C-MAST (Center for Mechanical and Aerospace Science and Technology), Research Unit No. 151 (Project UID/00151/2020). The authors also thank the Fundação para a Ciência e a Tecnologia (FCT), Fundo Social Europeu (FSE) and Programa Operacional Regional Centro 2020 and Norte 2020 for the strategic funding UID/FIS/04650/2020 and the grant SFRH/BPD/117838/2016 (J.N.P.).

References

[1] Y. Cao, W. Tan, Z. Wu, Aircraft icing: an ongoing threat to aviation safety, Aerosp. Sci. Technol. 75 (2018) 353–385, https://doi.org/10.1016/j.ast.2017.12.028
[2] K. Wei, Y. Yang, H. Zuo, D. Zhong, A review on ice detection technology and ice elimination technology for wind turbine, Wind Energy 23 (2020) 433–457, https://doi.org/10.1002/we.2427
[3] F.F. Rodrigues, M. Abdollahzadeh, J. Pascoa, L. Pires, Influence of exposed electrode thickness on plasma actuators performance for coupled deicing and flow control applications, Am. Soc. Mech. Eng. Fluids Eng. Div. FEDSM (2021), https://doi.org/10.1115/FEDSM2021-65728 FEDSM2021-65728, V003T05A004.
[4] R. Tirumala, N. Benard, E. Moreau, M. Fenot, G. Lalizel, E. Dorignac, Temperature characterization of dielectric barrier discharge actuators: influence of electrical and geometric parameters, J. Phys. D Appl. Phys. 47 (2014) 255203.
[5] F. Rodrigues, J. Pascoa, M. Trancossi, Heat generation mechanisms of DBD plasma actuators, Exp. Therm. Fluid Sci. 90 (2018) 55–65, https://doi.org/10.1016/j.expthermflusci.2017.09.005
[6] F.F. Rodrigues, J.N. Pereira, M. Abdollahzadeh, J. Pascoa, S.L. Mendez, Comparative evaluation of dielectric materials for plasma actuators active flow control and heat transfer applications, Am. Soc. Mech. Eng. Fluids Eng. Div. FEDSM (2021), https://doi.org/10.1115/FEDSM2021-65748 FEDSM2021-65748, V003T05A015.
[7] M. Abdollahzadeh, J.C. Pascoa, P.J. Oliveira, Comparison of DBD plasma actuators flow control authority in different modes of actuation, Aerosp. Sci. Technol. 78 (2018) 183–196, https://doi.org/10.1016/j.ast.2018.04.013
[8] J. Nunes-Pereira, F.F. Rodrigues, M. Abdollahzadehsangroudi, J.C. Páscoa, S. Lanceros-Mendez, Improved performance of polyimide cirlex-based dielectric barrier discharge plasma actuators for flow control, Polym. Adv. Technol. (2021) 1–13, https://doi.org/10.1002/PAT.5600
[9] J. Cai, Y. Tian, X. Meng, X. Han, D. Zhang, An experimental study of icing control using DBD plasma actuator, Exp. Fluids 58 (2017) 102–110, https://doi.org/10.1007/s00348-017-2378-y
[10] W. Zhou, Y. Liu, H. Hu, Utilization of thermal effect induced by plasma generation for aircraft icing mitigation, AIAA J. 56 (2018) 1097–1104, https://doi.org/10.2514/1.J056358
[11] Y. Liu, C. Kolbakir, H. Hu, H. Hu, A comparison study on the thermal effects in DBD plasma actuation and electrical heating for aircraft icing mitigation, Int. J. Heat Mass Transf. 124 (2018) 319–330, https://doi.org/10.1016/j.ijheatmasstransfer.2018.03.076
[12] X. Meng, H. Hu, C. Li, A.A. Abbasi, J. Cai, H. Hu, Mechanism study of coupled aerodynamic and thermal effects using plasma actuation for anti-icing, Phys. Fluids 31 (2019) 1–13, https://doi.org/10.1063/1.5086884

[13] C. Kolbakir, H. Hu, Y. Liu, H. Hu, A hybrid anti-/de-icing strategy by combining NS-DBD plasma actuator and superhydrophobic coating for aircraft icing mitigation, AIAA Scitech 2019 Forum 2019, p. 0050, doi: 10.2514/6.2019-0050.
[14] X. Zheng, H. Song, D. Bian, H. Liang, H. Zong, Z. Huang, Y. Wang, W. Xu, A hybrid plasma de-icing actuator by using SiC hydrophobic coating-based quartz glass as barrier dielectric, J. Phys. D Appl. Phys. 54 (2021) 375202, https://doi.org/10.1088/1361-6463/ac0bd8
[15] L. Guoqiang, Y. Shihe, Large eddy simulation of dynamic stall flow control for wind turbine airfoil using plasma actuator, Energy 212 (2020) 118753, https://doi.org/10.1016/J.ENERGY.2020.118753
[16] M.G. De Giorgi, V. Motta, A. Suma, Influence of actuation parameters of multi-DBD plasma actuators on the static and dynamic behaviour of an airfoil in unsteady flow, Aerosp. Sci. Technol. 96 (2020) 105587, https://doi.org/10.1016/J.AST.2019.105587
[17] W. Xu, Y. Wang, S. Huang, C. Li, Numerical study on plasma excitation flow control of Savonius vertical axis wind turbine, Energy 239 (2021) 122133, https://doi.org/10.1016/J.ENERGY.2021.122133
[18] M. Abdollahzadeh, J.C. Páscoa, P.J. Oliveira, Numerical investigation on efficiency increase in high altitude propulsion systems using plasma actuators, ECCOMAS 2012 Eur. Congr. Comput. Methods Appl. Sci. Eng. (2012) 6563–6581.
[19] S.G. Pouryoussefi, M. Mirzaei, F. Alinejad, S.M. Pouryoussefi, Experimental investigation of separation bubble control on an iced airfoil using plasma actuator, Appl. Therm. Eng. 100 (2016) 1334–1341, https://doi.org/10.1016/j.applthermaleng.2016.02.133
[20] M. Abdollahzadeh, F. Rodrigues, J.C. Pascoa, Simultaneous ice detection and removal based on dielectric barrier discharge actuators, Sens. Actuators A Phys. 315 (2020) 112361, https://doi.org/10.1016/j.sna.2020.112361
[21] M. Abdollahzadehsangroudi, J.C. Pascoa Marques, F.M. Freire Rodrigues. Ice detection /protection and flow control system based on printing of dielectric barrier discharge sliding plasma actuators. US20190193863A1, 2019.
[22] F. Rodrigues, M. Abdollahzadeh, J.C. Pascoa, P.J. Oliveira, An experimental study on segmented-encapsulated electrode dielectric-barrier-discharge plasma actuator for mapping ice formation on a surface: a conceptual analysis, J. Heat. Transf. 143 (2021) 011701, https://doi.org/10.1115/1.4048252
[23] J. Kriegseis, S. Grundmann, C. Tropea, Power consumption, discharge capacitance and light emission as measures for thrust production of dielectric barrier discharge plasma actuators, J. Appl. Phys. 110 (1) (2011) 013305, https://doi.org/10.1063/1.3603030
[24] F.F. Rodrigues, J.C. Pascoa, M. Trancossi, Experimental thermal characterization of DBD plasma actuators, ASME Int Mech. Eng. Congr. Expo. Proc. (2018) 1, https://doi.org/10.1115/IMECE2017-70541
[25] M.M. Wojewodka, C. White, K. Kontis, Effect of permittivity and frequency on induced velocity in ac-DBD surface and channel plasma actuators, Sens. Actuators A Phys. 303 (2020) 111831, https://doi.org/10.1016/J.SNA.2020.111831
[26] F. Rodrigues, J.C. Pascoa, M. Trancossi, Experimental analysis of alternative dielectric materials for DBD plasma actuators, Proc. ASME 2018 Int. Mech. Eng. Congr. Expo. (2018) 1–19, https://doi.org/10.1115/IMECE2018-87455
[27] E. Pescini, D.S. Martínez, M.G. De Giorgi, A. Ficarella, Optimization of micro single dielectric barrier discharge plasma actuator models based on experimental velocity and body force fields, Acta Astronaut. 116 (2015) 318–332, https://doi.org/10.1016/J.ACTAASTRO.2015.07.015
[28] M. Forte, J. Jolibois, J. Pons, E. Moreau, G. Touchard, M. Cazalens, Optimization of a dielectric barrier discharge actuator by stationary and non-stationary measurements of the induced flow velocity: application to airflow control, Exp. Fluids 43 (2007) 917–928, https://doi.org/10.1007/S00348-007-0362-7
[29] P. Mohammadpour, M. Mani, M. Saeedi, Experimental investigation of induced velocity by dielectric barrier discharge plasma actuator in different configurations, AIP Adv. 11 (2021) 105007, https://doi.org/10.1063/5.0057284
[30] F.F. Rodrigues, J.C. Pascoa, Implementation of stair-shaped dielectric layers in micro- and macroplasma actuators for increased efficiency and lifetime, J. Fluids Eng. 142 (2020) 104502, https://doi.org/10.1115/1.4047800

Mohammadmahdi Abdollahzadehsangroudi (M. Abdollahzadeh) received his Ph.D. in mechanical engineering from Universidade da Beira Interior in Portugal, in 2015. He is currently Post-Doctoral Researcher in the Center for Mechanical and Aerospace Sciences and Technologies of the Universidade da Beira Interior. His Research interest is Computational Fluid dynamics, Flow control and Energy systems.

Frederico Rodrigues received his Ph.D. in mechanical engineering from Universidade da Beira Interior in Portugal, in 2019. He is currently Post-Doctoral Researcher in the Center for Mechanical and Aerospace Sciences and Technologies of the Universidade da Beira Interior. His research interests are experimental fluid mechanics, electrohydrodynamic, thermo-fluid dynamics, plasma physics and aerodynamics.

João Nunes-Pereira received the Ph.D. degree in Physics in 2013 from the University of Minho, Braga, Portugal. Since 2014 he develops post-doctoral research activity at the Center of Physics of the Universities of Minho and Porto and at the Centre for Mechanical and Aerospace Science and Technologies at the University of Beira Interior, Covilhã, Portugal. His work is focused on the design, production, characterization and application of polymers and composites, especially smart and functional materials for sensors and actuators, energy systems, environmental remediation, and biomedical applications.

José Páscoa is currently Vice-Rector and Full professor at Universidade da Beira Interior. His Research interest is on Computational fluid dynamics, Energy and Multi-physics problems. with applications ranging from turbomachinery aerodynamics of cyclorotors, to magnetohydrodynamics, and eletrohydrodynamics of plasma actuators, electrostatic paint devices and electrospray thrusters.

Luís Carlos Carvalho Pires is an assistant professor at the Electromechanical Engineering Department at Universidade da Beira Interior and he is currently the Director of the Universidade da Beira Interior Library. His Research interest is on Thermal Energy Systems and Renewable Energies, more specifically in passive, or low energy, heating and cooling technologies, solar energy systems and thermography application in engineering and biomedical science.